# Advanced Modular Power System Electronics Enclosure Thermal Testing

*Anthony J. Colozza*
*Vantage Partners, LLC, Brook Park, Ohio*

*Brent G. Gardner*
*Glenn Research Center, Cleveland, Ohio*

# NASA STI Program . . . in Profile

Since its founding, NASA has been dedicated to the advancement of aeronautics and space science. The NASA Scientific and Technical Information (STI) Program plays a key part in helping NASA maintain this important role.

The NASA STI Program operates under the auspices of the Agency Chief Information Officer. It collects, organizes, provides for archiving, and disseminates NASA's STI. The NASA STI Program provides access to the NASA Technical Report Server—Registered (NTRS Reg) and NASA Technical Report Server—Public (NTRS)  thus providing one of the largest collections of aeronautical and space science STI in the world. Results are published in both non-NASA channels and by NASA in the NASA STI Report Series, which includes the following report types:

- TECHNICAL PUBLICATION. Reports of completed research or a major significant phase of research that present the results of NASA programs and include extensive data or theoretical analysis. Includes compilations of significant scientific and technical data and information deemed to be of continuing reference value. NASA counter-part of peer-reviewed formal professional papers, but has less stringent limitations on manuscript length and extent of graphic presentations.

- TECHNICAL MEMORANDUM. Scientific and technical findings that are preliminary or of specialized interest, e.g., "quick-release" reports, working papers, and bibliographies that contain minimal annotation. Does not contain extensive analysis.

- CONTRACTOR REPORT. Scientific and technical findings by NASA-sponsored contractors and grantees.

- CONFERENCE PUBLICATION. Collected papers from scientific and technical conferences, symposia, seminars, or other meetings sponsored or co-sponsored by NASA.

- SPECIAL PUBLICATION. Scientific, technical, or historical information from NASA programs, projects, and missions, often concerned with subjects having substantial public interest.

- TECHNICAL TRANSLATION. English-language translations of foreign scientific and technical material pertinent to NASA's mission.

For more information about the NASA STI program, see the following:

- Access the NASA STI program home page at http://www.sti.nasa.gov

- E-mail your question to help@sti.nasa.gov

- Fax your question to the NASA STI Information Desk at 757-864-6500

- Telephone the NASA STI Information Desk at 757-864-9658

- Write to:
  NASA STI Program
  Mail Stop 148
  NASA Langley Research Center
  Hampton, VA 23681-2199

NASA/TM—2019-220011

# Advanced Modular Power System Electronics Enclosure Thermal Testing

*Anthony J. Colozza*
*Vantage Partners, LLC, Brook Park, Ohio*

*Brent G. Gardner*
*Glenn Research Center, Cleveland, Ohio*

National Aeronautics and
Space Administration

Glenn Research Center
Cleveland, Ohio 44135

May 2019

*Level of Review*: This material has been technically reviewed by technical management.

Available from

This report is available in electronic form at http://www.sti.nasa.gov/ and http://ntrs.nasa.gov/

# Advanced Modular Power System Electronics Enclosure Thermal Testing

Anthony J. Colozza
Vantage Partners, LLC
Brook Park, Ohio 44142

Brent G. Gardner
National Aeronautics and Space Administration
Glenn Research Center
Cleveland, Ohio 44135

## Summary

An analysis was set up to model the temperature of the advanced modular power system (AMPS) power distribution cards when installed within the electronics enclosure case. The analysis was used to determine the steady-state temperature distribution of the cards within the case. To verify the analysis, an experiment was set up and conducted to simulate the operation of the cards within the enclosure. Four tests were conducted. The tests varied the position of the cold plate and evaluated the use of a thermal compound to reduce the contact resistance between the joints within the thermal path between the cards and the cold plate. Three of the four cases examined showed very good agreement between the analysis and the experiment with a less than 1-percent variation in the predicated temperatures determined through the analysis and the experimentally derived temperatures. In the remaining case, the difference between the analysis and experiment was approximately 12 percent. Both the experiment and analysis showed that the modular power conditioning cards can be maintained within their desired maximum operating temperature range of 40 to 45 °C through thermal conduction to a cold plate when operating with their estimated maximum heat output of 16 W per card.

## 1.0 Introduction

The advanced modular power system (AMPS) components consist of a number of standardized power conditioning and control cards that are housed in a card enclosure. The objective of the AMPS power conditioning card designs is to be modular and interchangeable, enabling them to be utilized in different locations and for conditioning output power for different types of loads. The AMPS architecture for spacecraft applications is intended to be a robust cost-savings approach to power system conditioning and control that provides inherent redundancy and reliability. The ability to utilize a single power condition card for a variety of load types and requirements enables

- A single card design to be produced, reducing cost
- A card to be moved from one location to another to address failures and ensure operation of critical loads
- A reduction in the number of spare cards required on the spacecraft since the single card design can be used for any of the spacecraft loads

To enable this modular approach to work, a standardized interface case is used with the cards to connect them to the loads. This card enclosure has a number of slots with a backplane that provides the input and output power interface as well as communication to the cards. The cards slide into the enclosure

and plug into the backplane. They are held in place with Wedgelock card retainers (Wakefield-Vette, Inc.) that mechanically expand to lock the cards against the side rails of the enclosure and hold them securely in place once installed.

The enclosures are regarded as part of the spacecraft structure and provide the electrical connections between the cards and the loads as well as the thermal control for the cards. The electrical and thermal connections to the enclosure are part of the infrastructure of the spacecraft. The final configuration will be dependent on the spacecraft design. However, for this initial evaluation, the cold plates used to remove the heat from the electronics enclosure are assumed to be located at either the rear or the top of the case. These locations represent the most likely configurations. However, if the enclosures are designed and installed as part of the spacecraft, then it may be possible that an integral cooling loop can be designed into the enclosures. This approach would provide the best heat removal capability, especially if the coolant loop can be integrated into the support rails that the cards are pressed against to hold them in place.

A custom enclosure was constructed to hold the cards for testing, as shown in Figure 1. This enclosure has the characteristics similar to that which is envisioned to be used in the spacecraft. Each enclosure is constructed of aluminum and can hold 17 cards in slots. The enclosures are stacked on top of each other in a rack.

Heat is generated from the electrical components and chips located on the printed circuit board (PCB). These heat sources are distributed over the board surface. Heat can be moved from these components to the enclosure through thermal planes located within or external to the board by contacting the surface of the chips or other components. Heat is then conducted to the case support rails and locking mechanism. The electronic components, the thermal planes, and their interface to the case is illustrated in Figure 2.

Once placed into a slot, the cards are locked into place with a Wedgelock card retainer that expands by using a sliding joint that expands outward as a screw is tightened, as shown in Figure 3. This compresses the card against the rails. This locking mechanism can provide good thermal contact between the card and the rails.



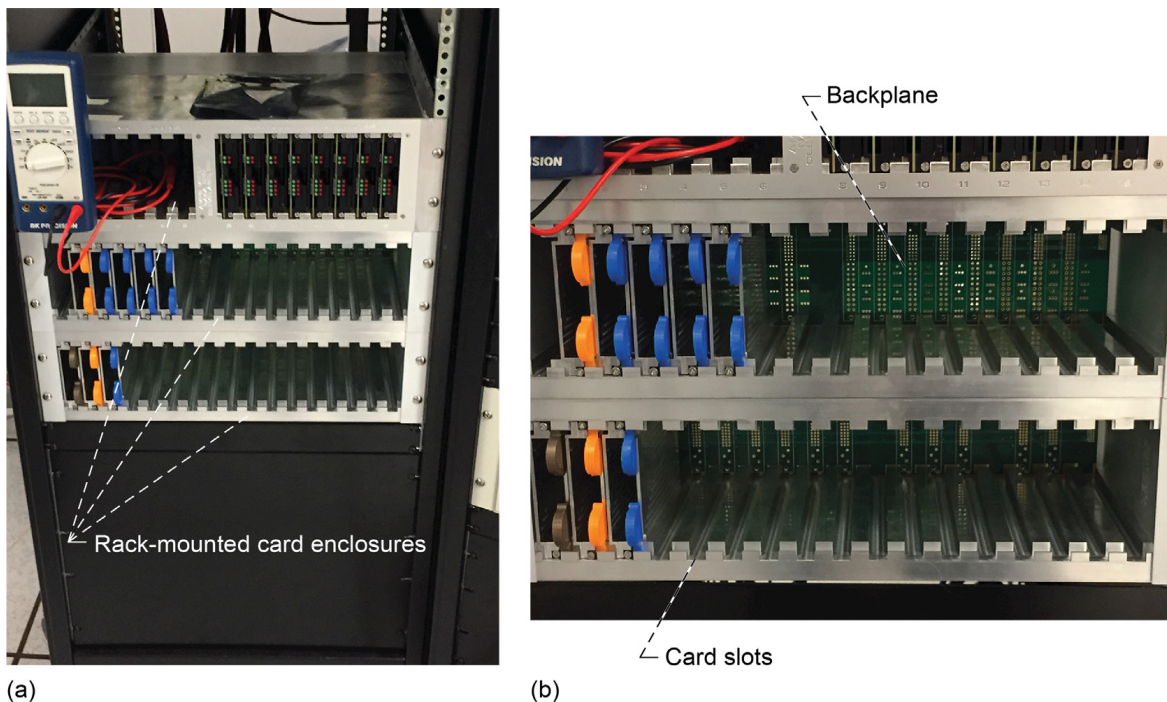(a)                                                                   (b)

Figure 1.—Card enclosures, card slots, and backplane. (a) Card enclosures mounted in rack. (b) Card slot and backplane locations.
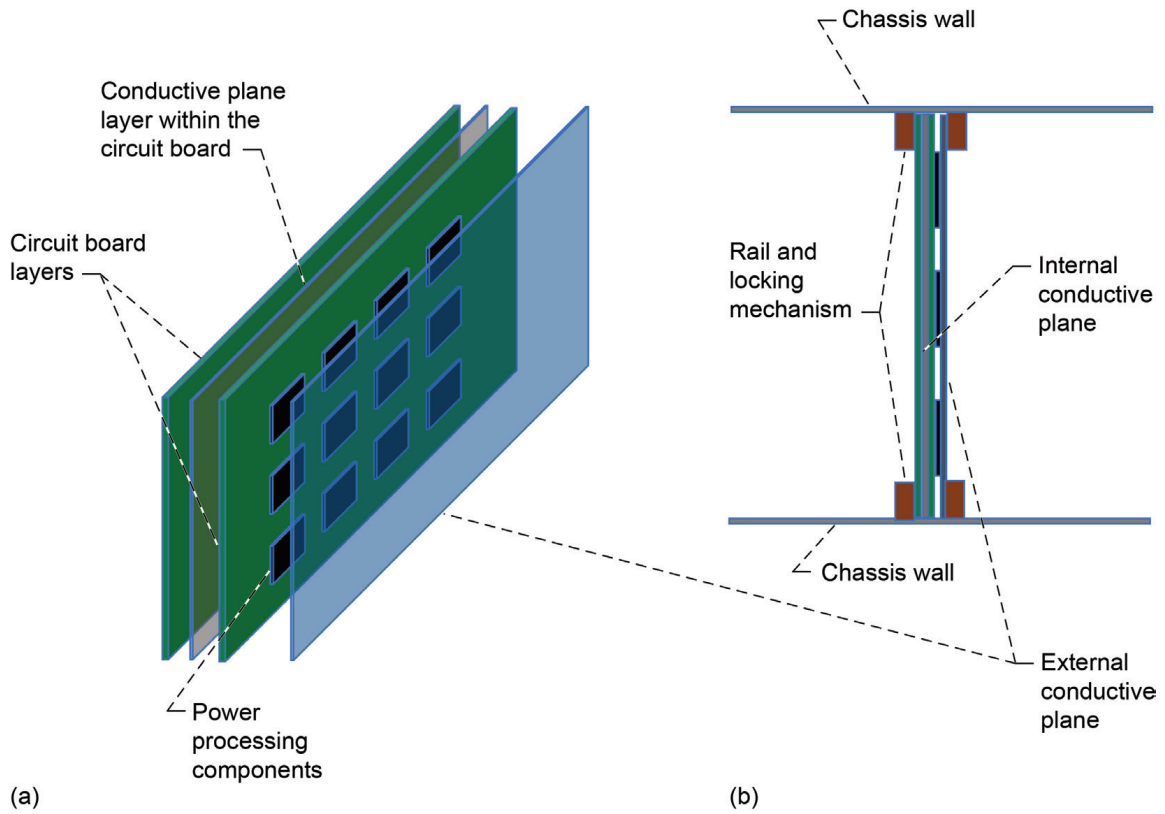
Figure 2.—Power conditioning card configuration. (a) Card components. (b) Card secured in slot.
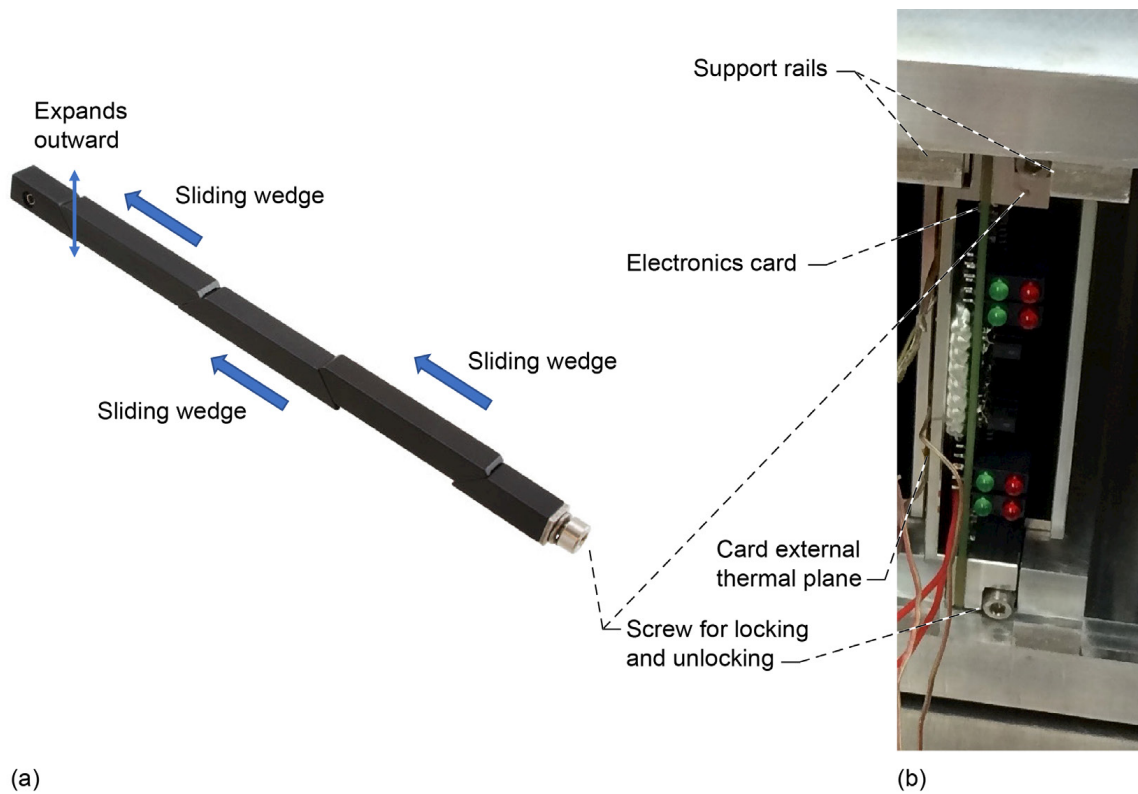


Figure 3.—Wedgelock printed circuit board card retainer. (a) Locking and unlocking screw. (b) Card secured in slot.

## 2.0 Analysis

An analytical model was set up to estimate the power conditioning card temperature with the cold plate mounted to the rear of the chassis. The heat flow from the card to the cold plate is illustrated in Figure 4. The chip temperature ($T_c$) is given by the sum of the thermal resistances between the chip surface and the heat sink ($R_{tot}$), the waste heat generated by the board ($P$), and the cold plate temperature ($T_s$), as given by Equation (1).

$$T_c = T_s + R_{tot}P \tag{1}$$

The total thermal resistance in degrees Kelvin per watt is a sum of the individual resistances associated with the heat path shown in Figure 4 and represented by Equation (2).

$$R_{tot} = R_{c,p} + R_p + R_{p,r} + R_r + R_{r,be} + R_{be} + R_{be,cp} \tag{2}$$

Heat initially moves from the electronics components to the external conductive thermal plane. The thermal plane conducts the heat to the rails and case, which in turn transports the heat to the cold plate located at the rear of the case. Because each rail, except for the rails associated with the ends of the case, is in contact with two cards, it was assumed that heat would flow from each card to two rails (one upper and one lower) and a portion of the case equivalent to the spacing between the cards. This minimizes the conduction for each card to the cold plate and represents a worst-case situation where all the cards are operational and each is producing the maximum amount of heat output allowed.

The thermal resistance for the heat flow from the electronics components to the conductive plane ($R_{c,p}$) in contact with their upper surface is given by Equation (3), which is based on the contact conductance between the electronic components and the thermal plane ($R_{c(c,p)}$) and the electronics components' contact area to the thermal plane ($A_c$).

$$R_{c,p} = \frac{R_{c(c,p)}}{A_c} \tag{3}$$

The thermal resistance for the heat conducted from the thermal plane to the upper and lower rails ($R_p$) is based on the average distance between the center of the thermal plane to the support rails ($d_p$), thermal plane thickness ($t_p$), thermal plane length ($L_p$), and thermal conductivity of the thermal plane ($k_p$), given by Equation (4).

$$R_p = \frac{d_p}{t_p k_p L_p} \tag{4}$$

The thermal resistance associated with the contact between the thermal plane and the support rail ($R_{p,r}$) is given by Equation (5), which is based on the contact conductance between the thermal plane and the support rails ($R_{c(p,r)}$) and the contact surface area between the two ($A_r$).
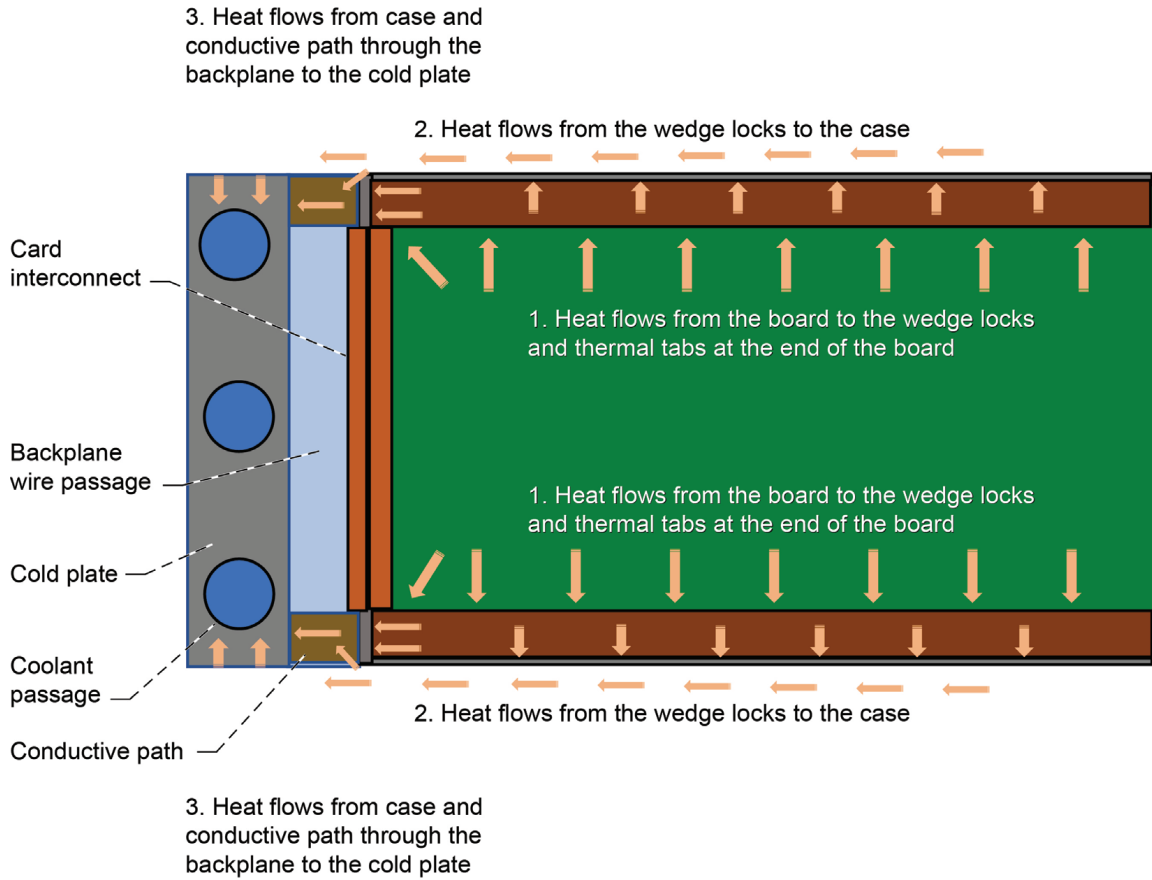
$$R_{p,r} = \frac{R_{c(p,r)}}{A_r} \tag{5}$$

Figure 4.—Heat flow illustration from electronics to rear-mounted cold plate.

The thermal resistance for the heat conducted down the rails and case to the backplane of the case ($R_r$) is based on the average distance of the backplane to the center of the electronics card ($d_r$), the cross-sectional area of the rails and portion of the case associated with the heat transfer from one card ($A_{rcs}$, given by Equation (6), where $w_r$ and $w_c$ are the width of the support rail and case section, respectively, and where $t_r$ and $t_c$ are the thickness of the support rail and case, respectively), and the thermal conductivity of the support rail and case ($k_r$), given by Equation (7).

$$A_{rcs} = w_r t_r + w_c t_c \qquad (6)$$

$$R_r = \frac{d_r}{A_{rcs} k_r} \qquad (7)$$

The thermal resistance associated with the contact between the support rail and case and the backplane extension ($R_{r,be}$) is given by Equation (8), which is based on the contact conductance between the support rails and the backplane extension ($R_{c(r,be)}$). The cross-sectional area for this interface is the same as that used in Equation (5).

$$R_{r,be} = \frac{R_{c(r,be)}}{A_{rcs}} \qquad (8)$$

The thermal resistance for the heat conducted through the backplane extension to the cold plate ($R_{be}$) is based on the backplane thermal extension length ($L_{be}$) given by Equation (9). The cross-sectional area and thermal conductivity of the backplane extension is the same as that used for the support rails and case in Equation (6).

$$R_{be} = \frac{L_{be}}{A_{rcs}k_r} \tag{9}$$

The thermal resistance associated with the contact between the backplane extension and the cold plate ($R_{be,cp}$) is given by Equation (10), which is based on the contact conductance between the backplane extension or support rails and the case and the cold plate ($R_{c(be,cp)}$). The cross-sectional area for this interface is the same as that used in Equation (5). This thermal resistance is also used between the support rails and case to the cold plate for the case where there is no backplane extension.

$$R_{be,cp} = \frac{R_{c(be,cp)}}{A_{rcs}} \tag{10}$$

The previously outlined analysis was used to determine the steady-state operating temperature of the board over a range of thermal power produced by the board during operation. The operating temperature was calculated for three cases.

In addition to the three cases where the cold plate was mounted at the rear of the case, an analysis was performed to evaluate the electronics temperature with the cold plate on the top of the case. For this case, the total thermal resistance is given by Equation (11).

$$R_{tot} = R_{c,p} + R_p + R_{p,r} + R_r + R_{r,cp} \tag{11}$$

With the cold plate on the top of the case, the thermal resistance associated with the conduction on the support rails and case is through their thickness as opposed to down their length as in the previous cases. This resistance is given by Equation (12), where the heat transfer cross-sectional area is given by Equation (13).

$$R_r = \frac{t_c}{2A_{rcs}k_r} \tag{12}$$

$$A_{rcs} = w_c L_p \tag{13}$$

The last term in Equation (11) is the contact resistance between the cold plate and the top of the case ($R_{r,cp}$). This is given by Equation (14), which is based on the contact conductance between the support rails and case to the cold plate ($R_{c(r,cp)}$). The cross-sectional area for this interface is the same as that used in Equation (13).

$$R_{r,cp} = \frac{R_{c(r,cp)}}{A_{rcs}} \tag{14}$$

The cases in this work are as follows:

- Case 1: the cold plate mounted to the end of the support rails before the backplane spacing.
- Case 2: the cold plate mounted to the end of the backplane extension with no thermal compound used between the backplane extension and the rails.
- Case 3: the cold plate mounted to the end of the backplane extension with thermal compound used between the backplane extension and the rails.
- Case 4: the cold plate is mounted to the top of the case.

The associated variables used for each of these cases are summarized in Table I.

By using the previous analysis, the electronics board operating temperature was calculated over a range of operating powers. These results are shown in Figure 5 for cases 1 through 4. The maximum desired operating temperature was given as 40 °C. The resulting board temperatures for the baseline operating power level of 16 W are given in Table II.

TABLE I.—VARIABLE VALUES USED FOR FOUR CASES EXAMINED

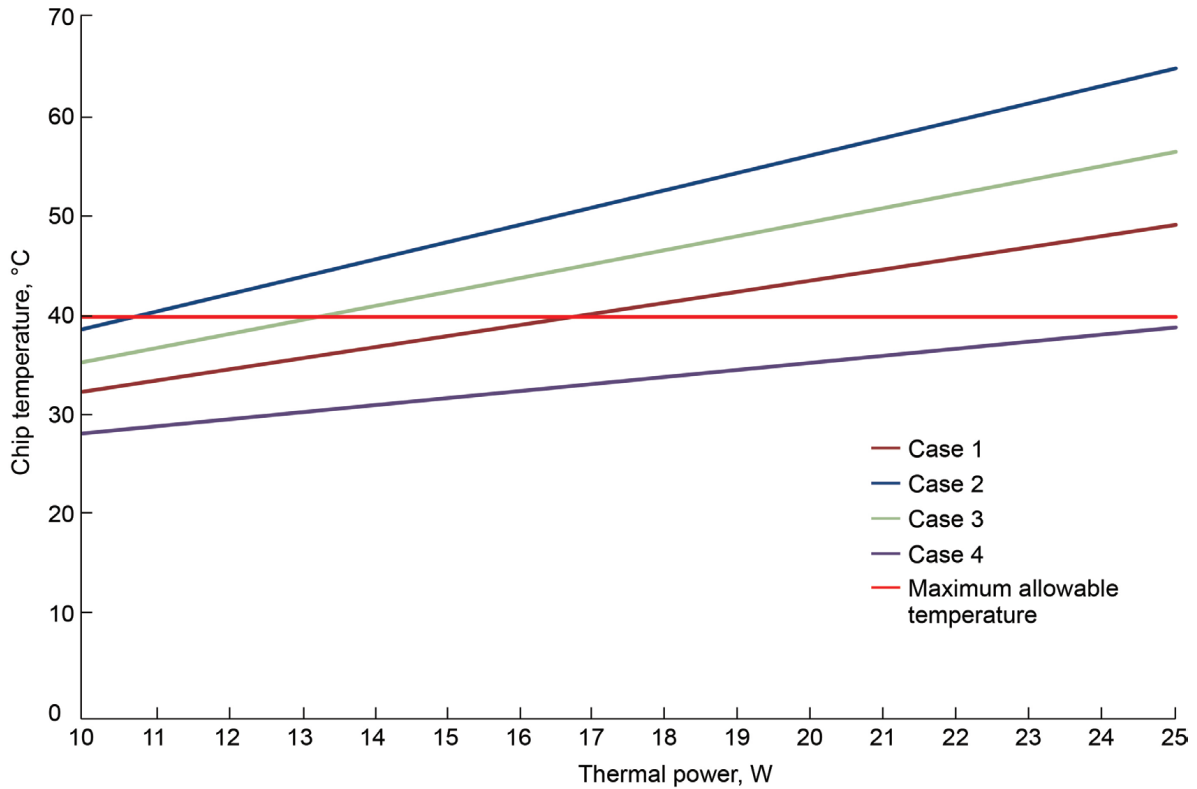| Variable | Case 1 | Case 2 | Case 3 | Case 4 |
|---|---|---|---|---|
| $A_c$ (electronics components' contact area to thermal plane), cm² | 82.6 | 82.6 | 82.6 | 82.6 |
| $A_r$ (contact area between thermal plane and support rail), cm² | 39.6 | 39.6 | 39.6 | 39.6 |
| $d_p$ (average distance from center of thermal plane to support rail), cm | 5.0 | 5.0 | 5.0 | 5.0 |
| $d_r$ (average distance from backplane to center of electronics card), cm | 8.2 | 8.2 | 8.2 | ------------ |
| $k_p$ (thermal conductivity of thermal plane), W/mK | 205 | 205 | 205 | 205 |
| $k_r$ (thermal conductivity of support rail and case), W/mK | 205 | 205 | 205 | 205 |
| $L_p$ (thermal plane length), cm | 16.5 | 16.5 | 16.5 | 16.5 |
| $L_{be}$ (backplane thermal extension length), cm | 0 | 10.8 | 10.8 | ------------ |
| $R_{c(be,cp)}$ (contact conductance between backplane extension or support rails and case and cold plate) (Ref. 1), m²K/W | 0.00036 | 0.00036 | 0.00036 | ------------ |
| $R_{c(c,p)}$ (contact conductance between electronic components and thermal plane), m²K/W | .0009 | .0009 | .0009 | 0.0009 |
| $R_{c(p,r)}$ (contact conductance between thermal plane and support rails) (Ref. 1), m²K/W | .00036 | .00036 | .00036 | .00036 |
| $R_{c(r,be)}$ (contact conductance between support rails and backplane extension) (Ref. 1), m²K/W | ------------ | .00036 | .0001429 | ------------ |
| $R_{c(r,cp)}$ (contact conductance between support rails and case to cold plate) (Ref. 1), m²K/W | ------------ | ------------ | ------------ | .00036 |
| $t_p$ (thermal plane thickness), mm | 3.0 | 3.0 | 3.0 | 3.0 |
| $t_c$ (thickness of case), mm | 15.6 | 15.6 | 15.6 | 15.6 |
| $t_r$ (thickness of support rail), °C | 8.5 | 8.5 | 8.5 | 8.5 |
| $T_s$ (cold plate temperature), °C | 21.5 | 21.5 | 21.5 | 21.5 |
| $w_c$ (width of case section), mm | 25.5 | 25.5 | 25.5 | 25.5 |
| $w_r$ (width of support rail), mm | 12.4 | 12.4 | 12.4 | 12.4 |

Figure 5.—Analysis results for board operating temperature for range of operating powers.

TABLE II.—ELECTRONICS BOARD
OPERATING TEMPERATURE AT 16 W

| Case | Operating temperature, °C |
|------|---------------------------|
| 1 | 39.2 |
| 2 | 49.1 |
| 3 | 43.9 |
| 4 | 32.7 |

This analysis shows that with the cold plate mounted on the rear of the case behind the backplane, the temperature of the board exceeded the desired 40 °C maximum temperature when operating with 16 W of waste heat per board. The addition of the Arctic Silver® (Arctic Silver, Inc.) thermal contact paste did lower the operating temperature 2.4 °C at the 16 W waste heat level. With the cold plate located inside the backplane, the operating temperature was at 37 °C, which is below the desired maximum. The best case was with the cold plate located on top of the electronics enclosure. In this case, the heat path to the cold plate is minimized and this results in the lowest calculated operating temperature of 31.8 °C. For case 4, the board operating temperature was below the maximum 40 °C temperature limit over the complete waste heat power level range (up to 25 W) that was considered.

## 3.0    Steady-State Temperature Experiment

To validate the thermal model and to provide additional insight into the effects of the cold plate interface to the electronics enclosure on the electronics temperature, an experiment was performed. The experiment was used to simulate the heat generated from an operational electronics card within the enclosure and determine its operating temperature. Four experiments were conducted by matching the four cases outlined in Section 2.0. In each of the experiments, four electronics cards were used. The cards were placed in the four slots toward the center of the 17-slot case, as shown in Figure 6.

The electronics cards used were representative of those that would be utilized in the operational power distribution unit (PDU) but were nonfunctional. They did have various electronics components on them and utilized an aluminum outer thermal plane as the operational cards would. To simulate their operation, flexible heaters were mounted on the inside of the thermal plane as shown in Figure 7.

Flexible strip heaters were used to simulate the operation of the cards and provide the desired waste heat to be removed by the cold plate. The heaters had a measured resistance of 154.6 $\Omega$. The heaters were wired in parallel and powered with a Sorensen DLM 60–10 power supply (AMETEK Programmable Power, Inc.), as illustrated in Figure 8. The output power of the supply to all of the heaters was 50.6 V at 1.31 A, providing a total of 66 W. This resulted in an output power of 16.6 W per heater. This power level was used as the baseline for all of the tests performed and was representative of the expected waste heat produced by the electronics cards.
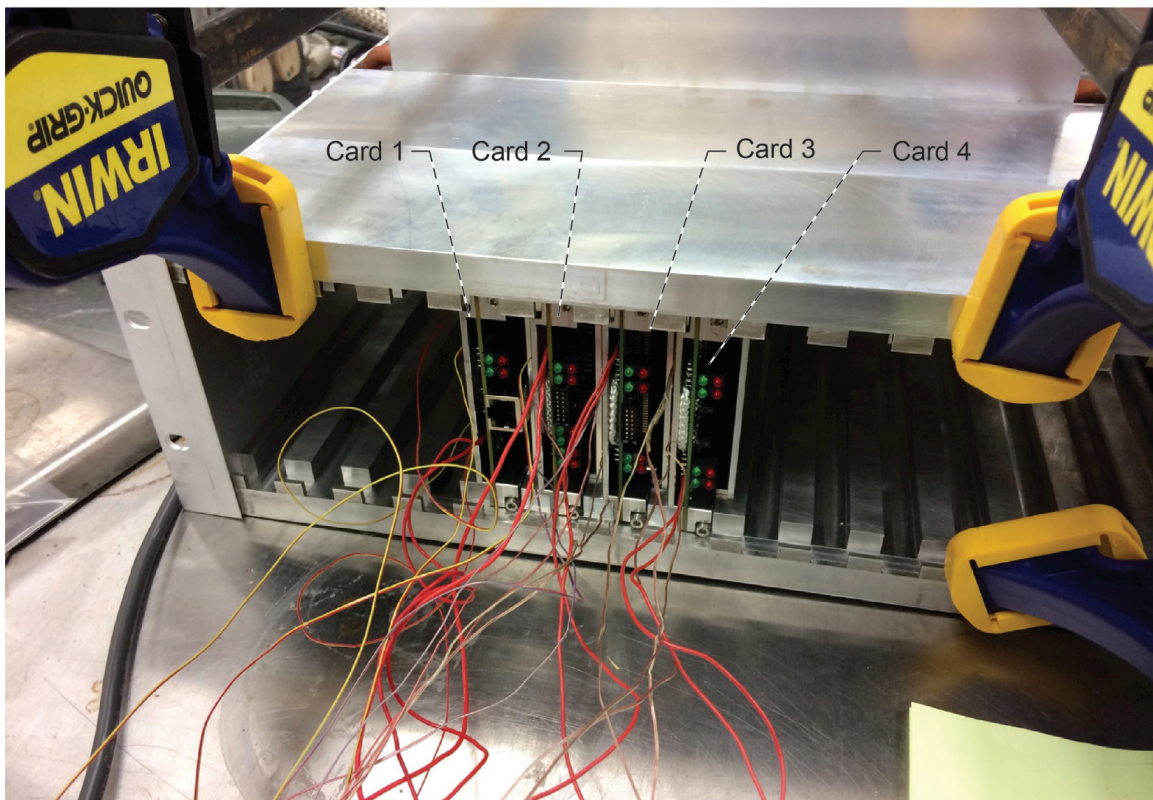


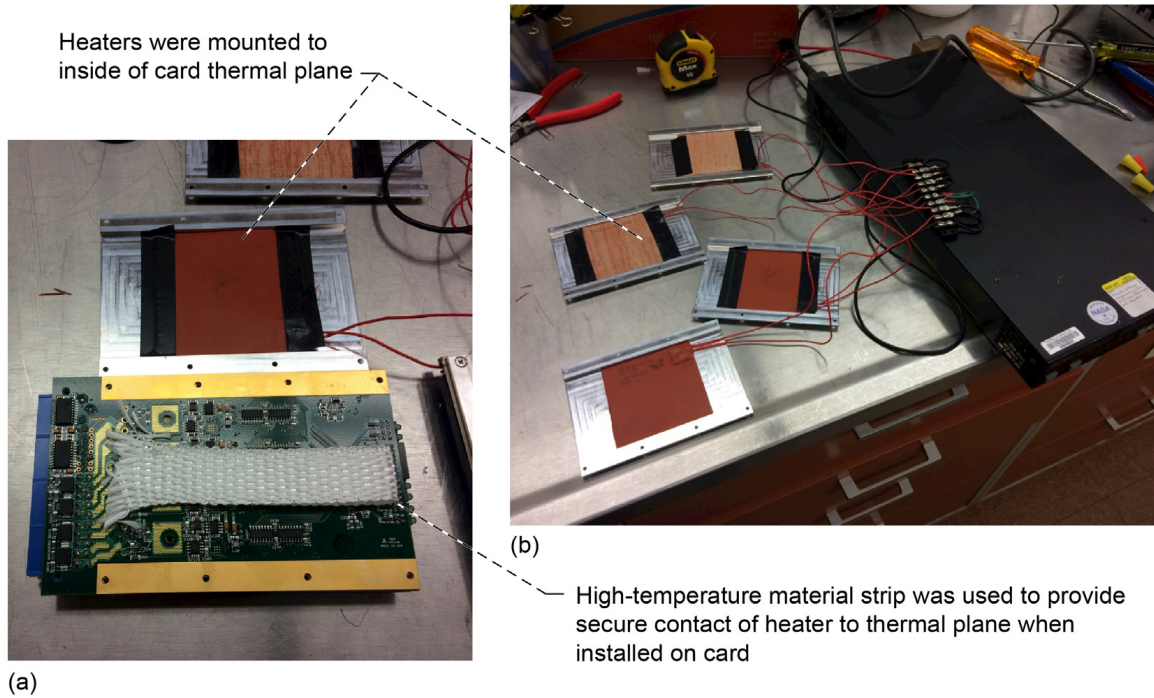Figure 6.—Test electronics cards installed in electronics enclosure.

Figure 7.—Electronics card heater installation. (a) High-temperature material strip installed on card. (b) Cards with heaters mounted to card thermal planes.
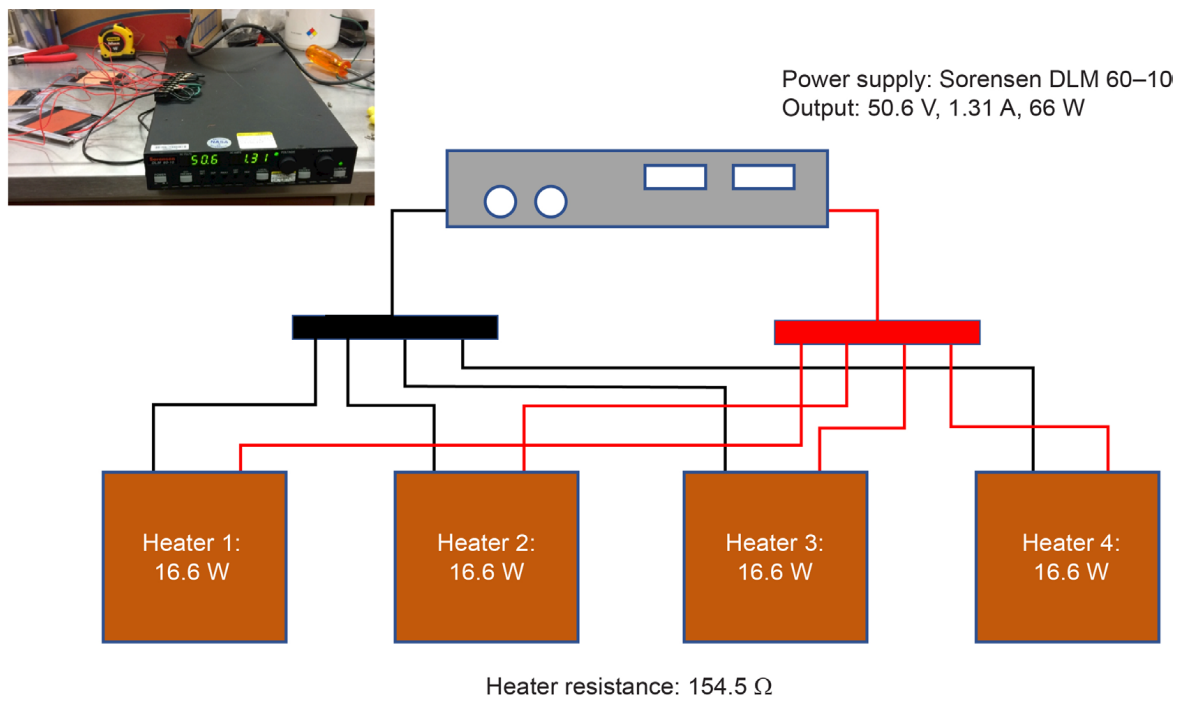


Figure 8.—Heater wiring and operational power level illustration.

The thermal plane on each of the cards was instrumented with four thermocouples spaced evenly over the surface, as shown in Figure 9. These thermocouples provided the card temperature during operation as well as showing any gradient in temperature over the card that may occur.

Thermocouples were also installed on the top of the electronics case and on the cold plate, as shown in Figure 10. The thermocouples on the top of the case were centered on the portion of the case where the cards were located. One was placed toward the front of the case and one toward the rear, closer to the cold plate placement during most of the testing. This thermocouple placement will show any temperature gradient that occurs in the case as the heat flows to the cold plate at the rear. The thermocouples on the cold plate were also centered on the card location. One was placed over the inlet flow tube and the second over the outlet flow tube. This placement will show the uniformity in temperature across the cold plate during operation. The thermocouples used were a combination of type T and K. The thermocouples were attached with an adhesive pad to the surface they were measuring.

A total of 20 thermocouples, between the four electronics cards, case, and cold plate, were used to monitor temperatures during the testing. Data from these thermocouples was recorded with a Graphtec GL820 data logger (Graphtec Corporation), as shown in Figure 11. The thermocouple channel input and corresponding location is given in Table III. The data logger was set to sample points from each thermocouple once a second. Data collection for each test was started prior to the power supply being turned on and continued until a steady-state temperature profile was achieved.
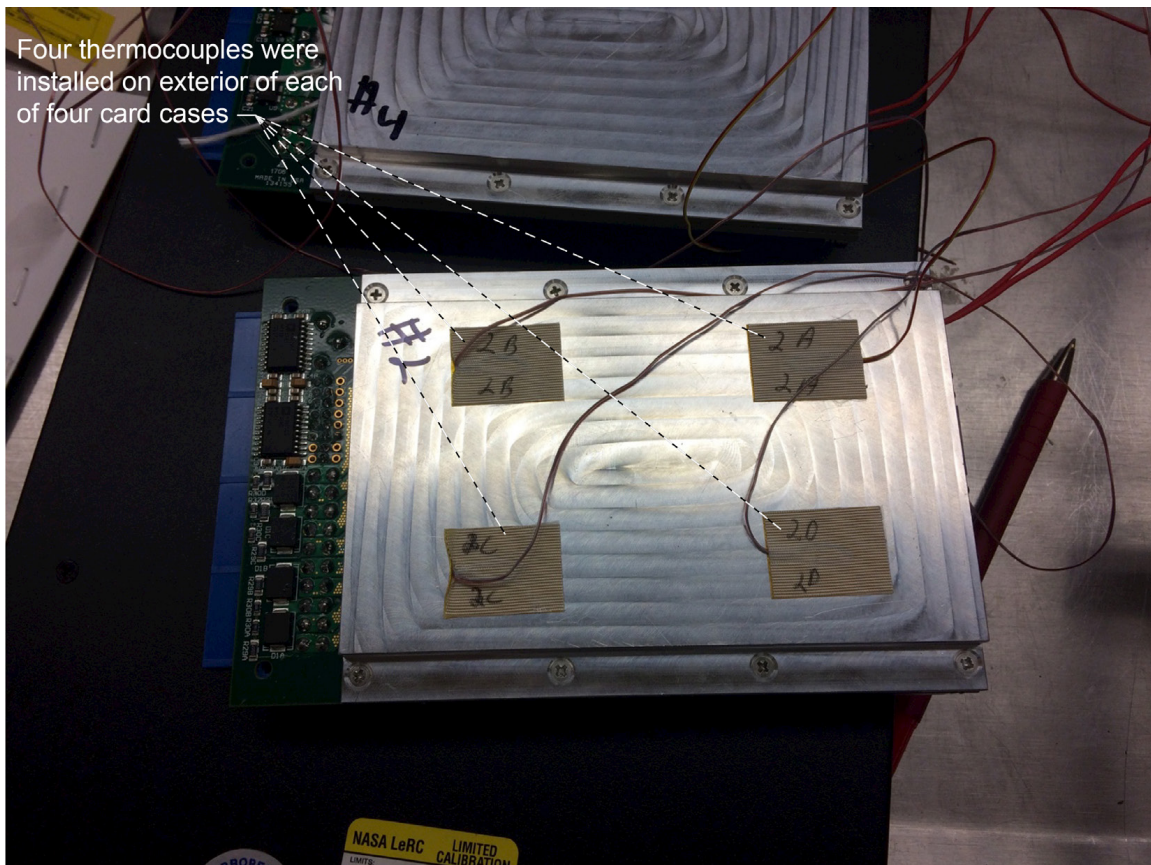


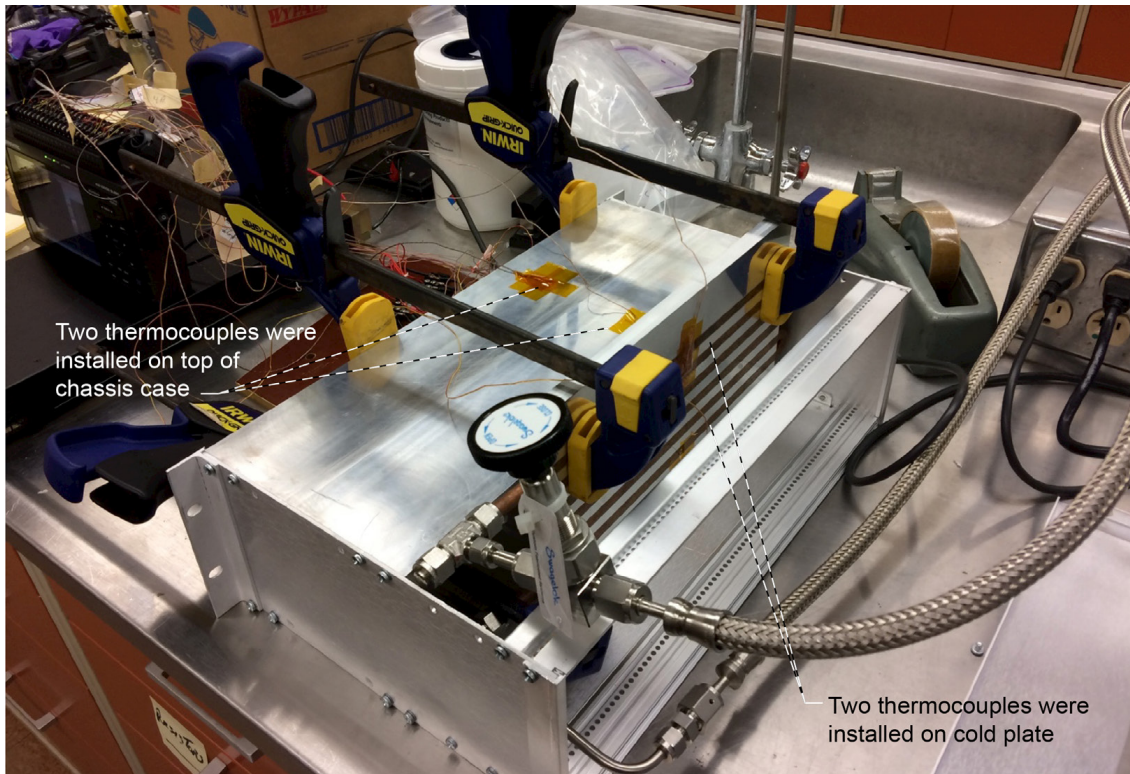Figure 9.—Thermocouple installation on electronics card thermal plane.

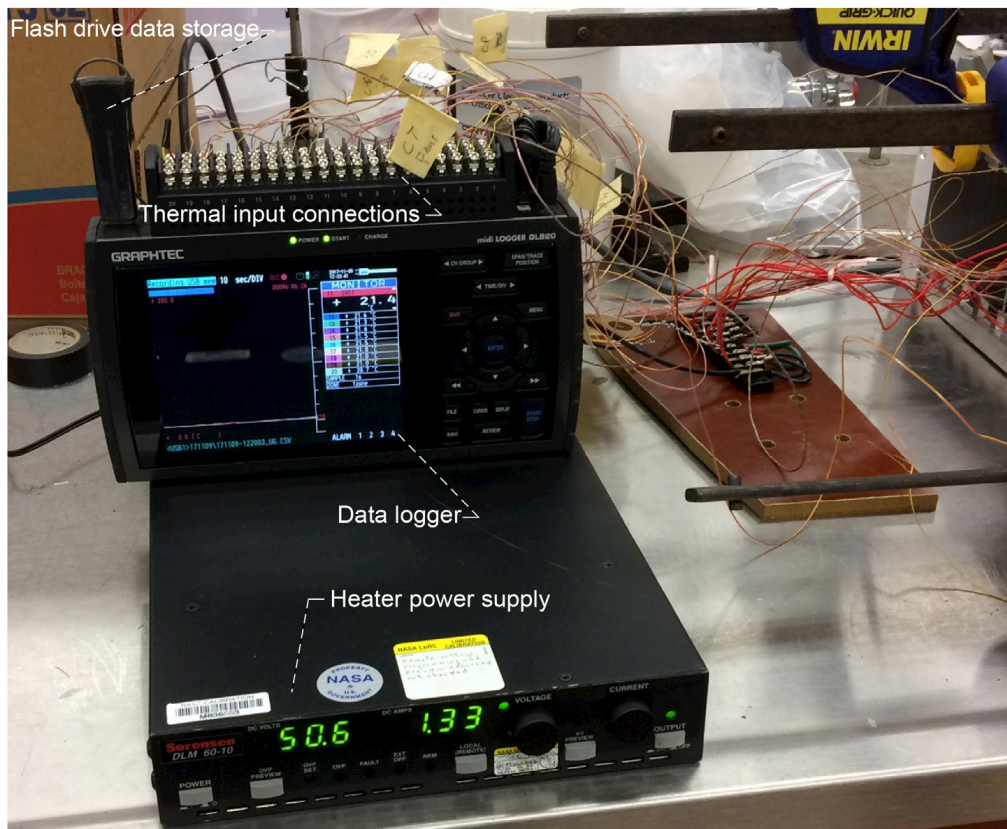Figure 10.—Thermocouple locations on case and cold plate.



Figure 11.—Thermocouple data acquisition.

TABLE III.—DATA LOGGER THERMOCOUPLE CHANNEL ASSIGNMENT

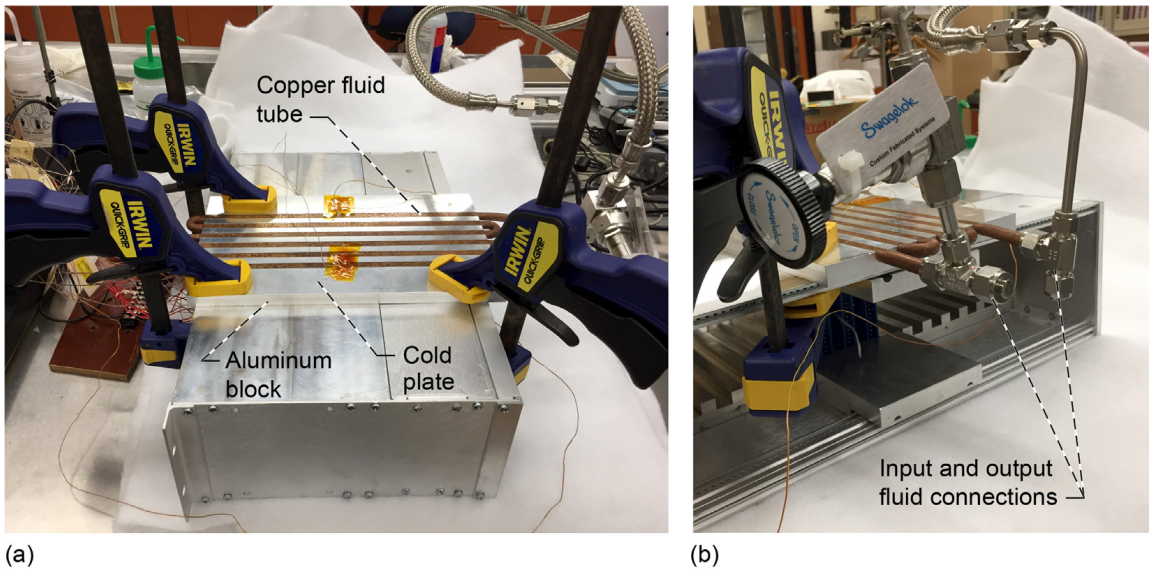| Channel | Location | Thermocouple type | Channel | Location | Thermocouple type |
|---------|----------|-------------------|---------|----------|-------------------|
| 1 | Card 1, top front | K | 11 | Card 3, bottom rear | K |
| 2 | Card 1, top rear | K | 12 | Card 3, bottom front | K |
| 3 | Card 1, bottom rear | K | 13 | Card 4, top front | K |
| 4 | Card 1, bottom front | K | 14 | Card 4, top rear | K |
| 5 | Card 2, top front | K | 15 | Card 4, bottom rear | K |
| 6 | Card 2, top rear | T | 16 | Card 4, bottom front | K |
| 7 | Card 2, bottom rear | T | 17 | Cold plate, bottom | K |
| 8 | Card 2, bottom front | T | 18 | Cold plate, top | K |
| 9 | Card 3, top front | T | 19 | Case, top rear | K |
| 10 | Card 3, top rear | T | 20 | Case, top front | K |



Figure 12.—Cold plate and fluid connections. (a) Cold plate mounted to enclosure. (b) Copper tube input and output connections.

The cold plate, which is used to remove heat from the electronics cards, was mounted to the enclosure by using adjustable clamps. This mounting approach was used for all three cold plate locations tested. The cold plate consists of an aluminum plate with an embedded serpentine copper tube through which the coolant flows. The cold plate is shown mounted to the top of the case in Figure 12.

A PolyScience 9102 (PolyScience) chiller was used to maintain the coolant flow at the desired setpoint temperature of 20 °C. The complete test layout is shown in Figure 13.

To reduce the convective heat transfer from the case and conduction into the test table, a polyester insulation was used to wrap the electronics case for testing. This insulation warp is shown in Figure 14.
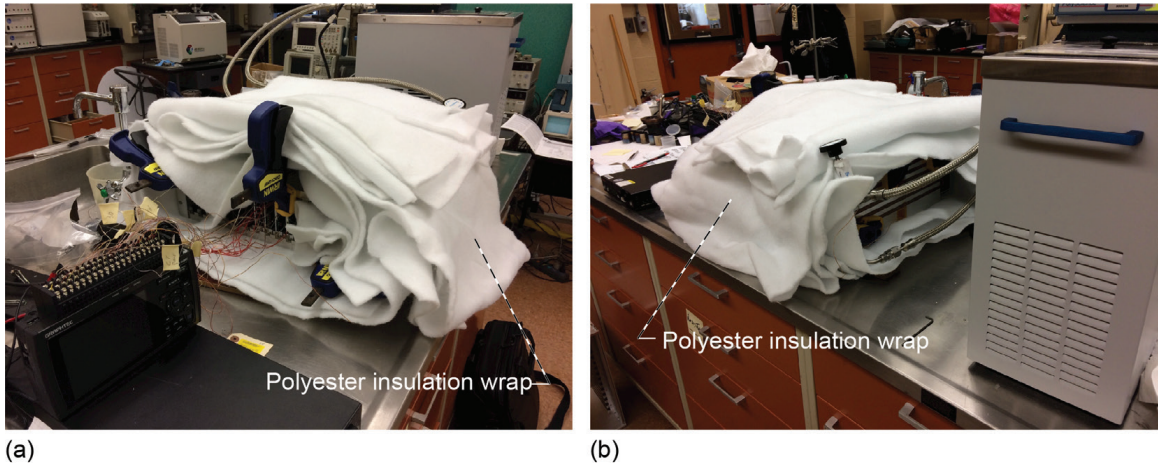
Figure 13.—Test setup.



(a)

(b)

Figure 14.—Electronics case wrapped with insulation. (a) Front view of insulation wrap installation. (b) Rear view of insulation wrap installation.
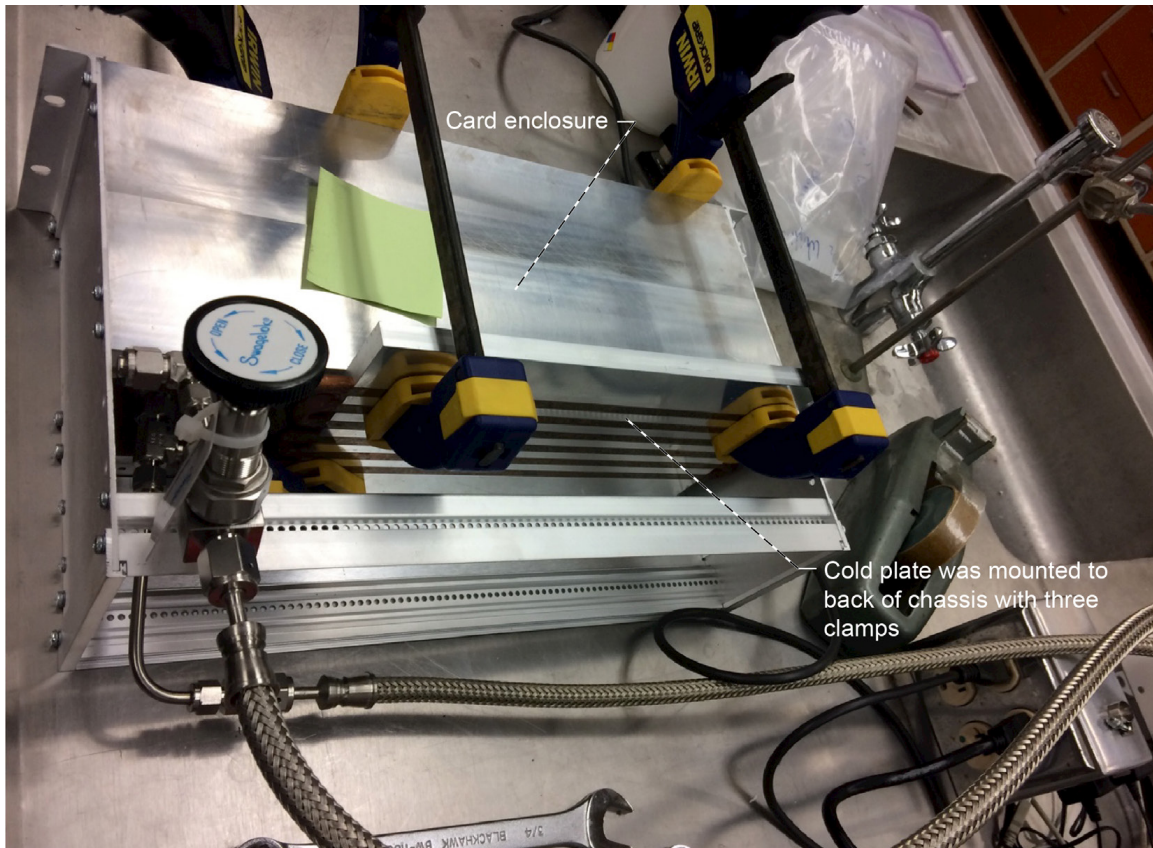
Figure 15.—Cold plate mounting location for case 1.

## 3.1 Case 1 Experimental Test Results

For case 1, the cold plate was located at the end of the support rails in the back of the card enclosure as shown in Figure 15. The test results for this case are shown in Figure 16 to Figure 19 for test cards A through D, respectively. The graphs show the rise in temperature of the cards over time as a constant heat load of 16.6 W per card is applied from the heaters.

The temperature distribution for all four cards reached a steady state after approximately 50 min. The average equalization temperature for each card is given in Table IV.

The temperature distribution of card A, given in Figure 16, showed that the bottom of the card was slightly cooler than the top of the card. This indicates that there was better heat flow through the bottom rail than the upper one. This is most likely due to variation in the surface finish between the upper and lower rails or the difference in the compressive force applied between the upper and lower Wedgelock card retainers. A higher compressive force will make better thermal contact, reducing the contact resistance, thereby enhancing the heat flow to that rail.

Card B did not show a similar distribution, but it did show a gradient between the front and rear of the card, as seen in Figure 17, where the front was warmer than the rear. This is to be expected since the front portion of the card is farther away from the cold plate than the rear.

For card C, shown in Figure 18, the temperature distribution for three of the thermocouples was very close, showing a slight increase in temperature between the front and rear of the card. However, the bottom rear thermocouple was reading significantly lower than the others. This is likely due to poor contact between the thermocouple and card thermal plane. Therefore, the output of this thermocouple was not used to calculate the card average temperature.
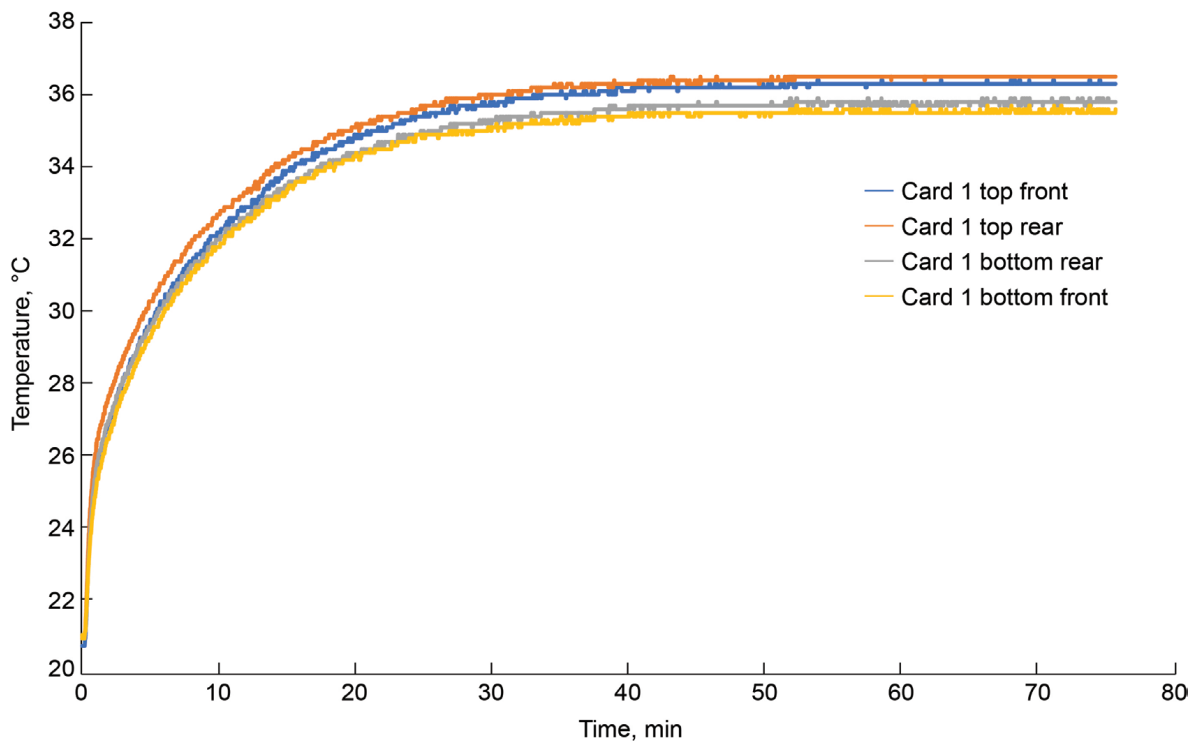
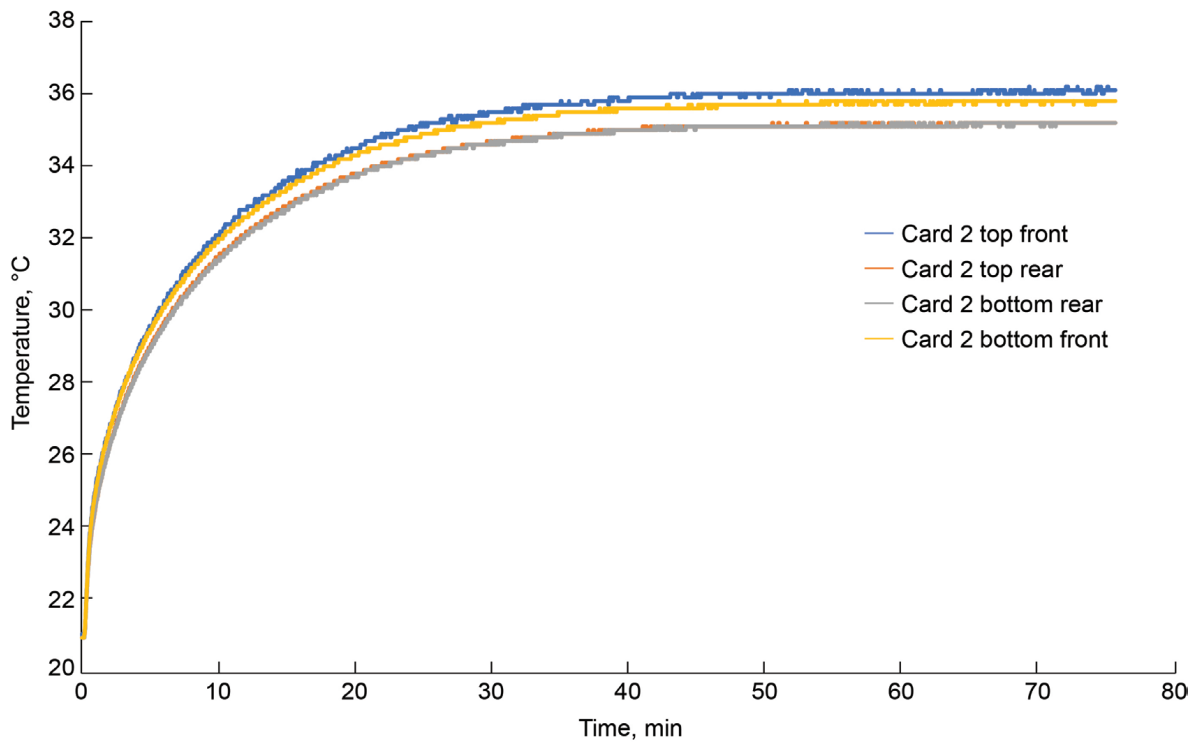Figure 16.—Case 1 card A temperature versus time.



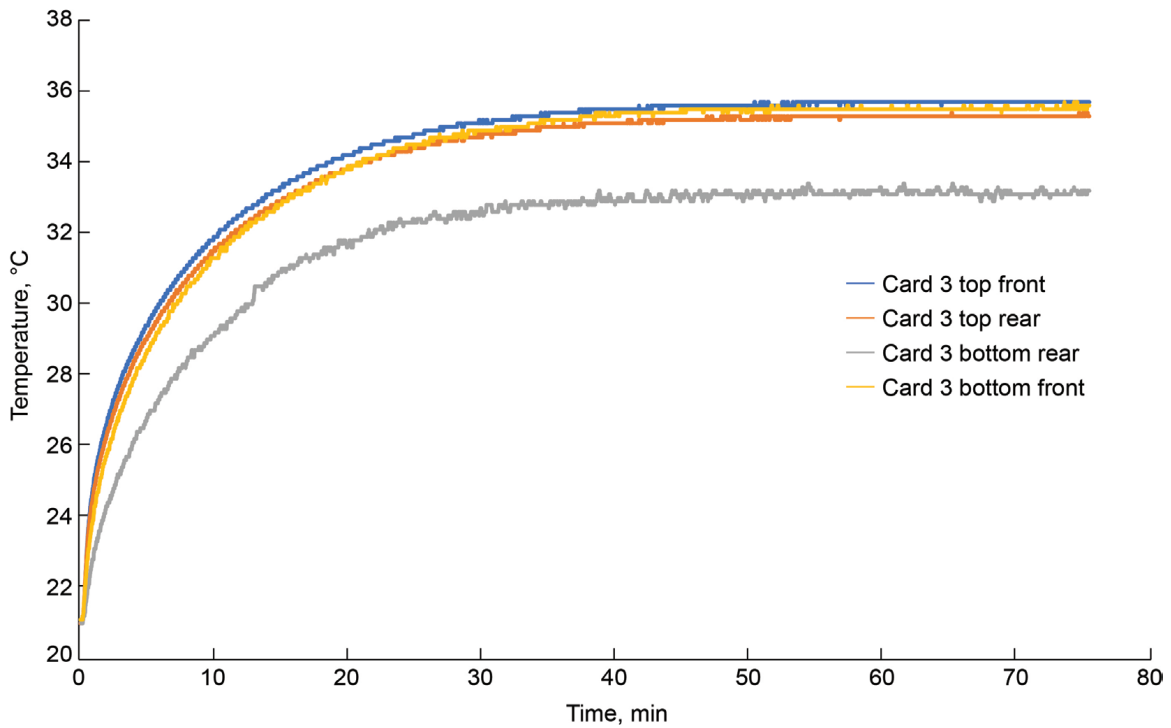Figure 17.—Case 1 card B temperature versus time.

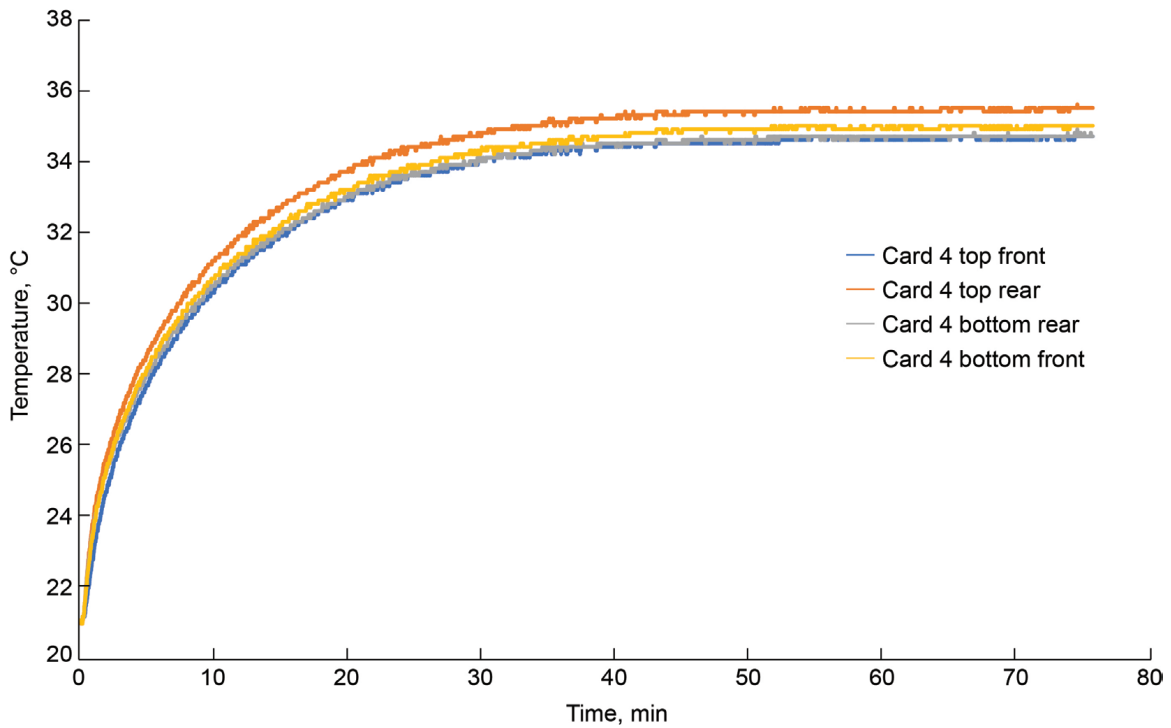Figure 18.—Case 1 card C temperature versus time.



Figure 19.—Case 1 card D temperature versus time.

For card D, shown in Figure 19, the top rear showed the highest temperature with the other three sites showing similar temperatures. As with card A, the variation between the top and bottom rear thermocouples is likely due to the difference in contact resistance between the upper and lower rails.

The temperatures of the cold plate and case were also monitored. These are shown in Figure 20 and the average values during steady-state temperature operation are shown in Table IV. There was a gradient of approximately 1 °C across the cold plate during steady-state operation, with an overall average operating temperature of 21.7 °C. The case had a 2 °C temperature variation between the front and rear (closer to the cold plate) with an overall average temperature of 30.0 °C.

TABLE IV.—CASE 1 AVERAGE
STEADY-STATE TEMPERATURES

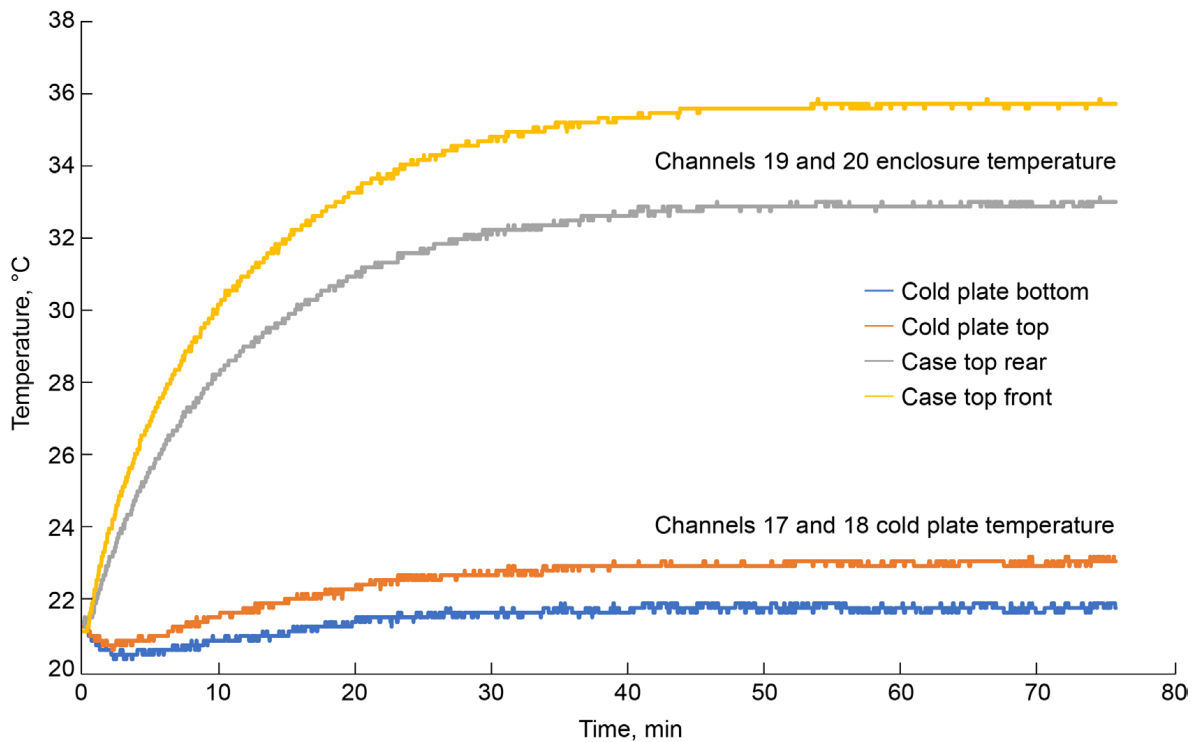| Location | Average equalization temperature, °C |
|---|---|
| Card A | 35.4 |
| Card B | 35.0 |
| Card C | 34.9 |
| Card D | 34.3 |
| Cold plate, bottom | 21.3 |
| Cold plate, top | 22.2 |
| Case, rear | 29.0 |
| Case, front | 31.0 |

Figure 20.—Case 1 enclosure and cold plate temperatures.

### 3.2    Case 2 Experimental Test Results

For case 2, the cold plate was located behind the backplane at the rear of the card enclosure as shown in Figure 21.

Since the enclosure walls around the backplane portion were thin, conductive blocks were added to effectively conduct heat across the backplane. These blocks were constructed of aluminum and installed at the top and bottom of the case in the location where the test cards were installed, as shown in Figure 22. The conductive blocks were wide enough to encompass the four card slots that were being used to generate the internal heat within the enclosure. These blocks provided nearly the same cross-sectional area as that of the rails and case for conducting heat across the backplane to the cold plate. They extended slightly beyond the edge of the enclosure to enable the cold plate to be securely pressed against them.

The test results for this case are shown in Figure 23 to Figure 26 for test cards A through D, respectively. The graphs show the rise in temperature of the cards over time as a constant heat load of 16.6 W per card from the heaters is applied. In case 1, the steady-state temperature distribution was reached after approximately 50 min, which was considerably less time than that needed for case 2. For case 2, the system had not reached a steady state after nearly 150 min of operation. The temperature data for all of the cards, case, and cold plate were beginning to level off when the test was ended. Therefore, to approximate the steady-state operating temperatures, curve fits of the data were made to extend the data out to 200 min, where the steady-state temperatures would have been reached. These curve fits of the data are shown on the graphs along with the equation for each fit.

The estimated steady-state temperature distribution for all four cards, the cold plate, and the case are given in Table V. These temperatures were generated with the data curve fit equations. The temperatures given for the individual cards were the average of the data from the four thermocouples on each card, extrapolated to 180 min by using the generated curve fits.
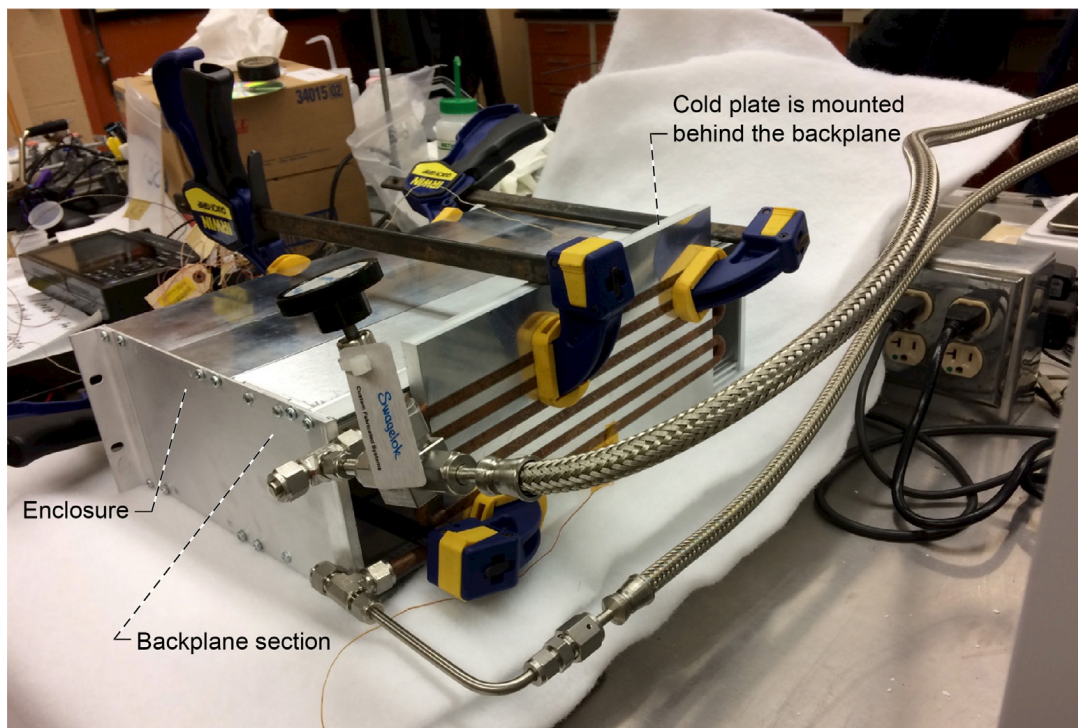
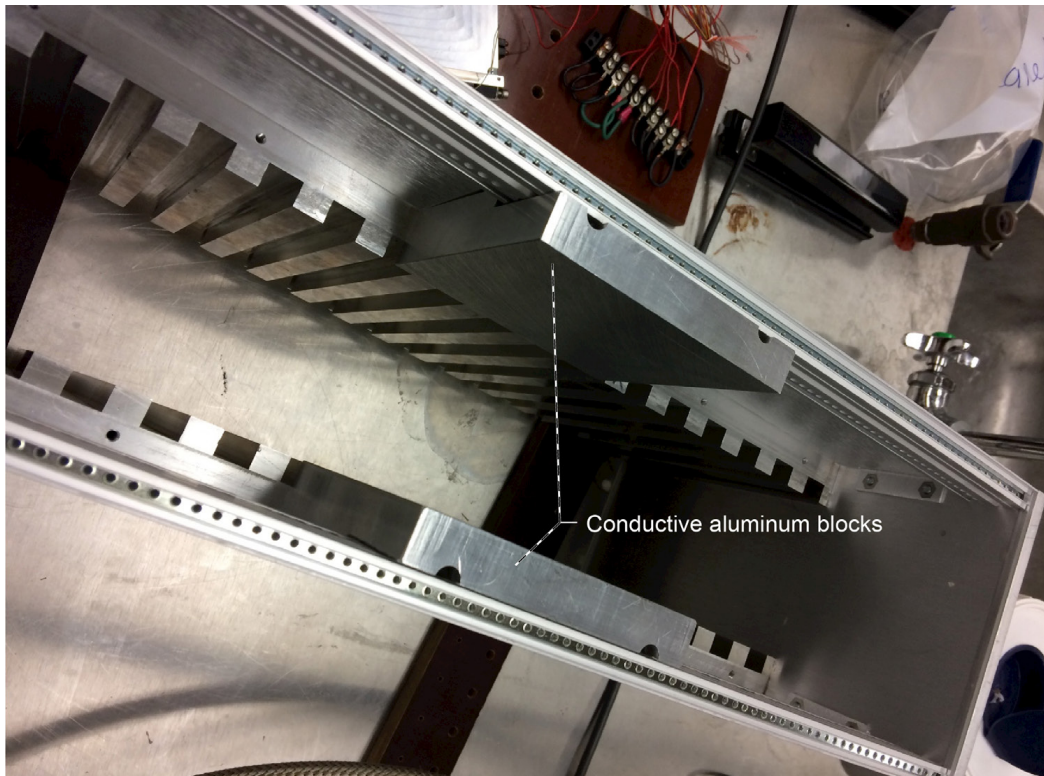

Figure 21.—Cold plate mounting location for case 2.

Figure 22.—Conductive aluminum blocks used to bridge backplane.

TABLE V.—CASE 2 AVERAGE
STEADY-STATE TEMPERATURES

| Location | Average equalization temperature, °C |
|---|---|
| Card A | 49.5 |
| Card B | 49.8 |
| Card C | 49.7 |
| Card D | 49.2 |
| Cold plate, bottom | 21.1 |
| Cold plate, top | 21.3 |
| Case, rear | 40.2 |
| Case, front | 46.4 |

The temperature distribution of card A, given in Figure 23, showed a fairly close temperature distribution over the card with about a 2 °C variation over the card surface. The coolest portion of the card was the bottom front, whereas the warmest portion was the top rear. As with the case 1 test, these results indicate that there was better heat flow through the bottom rail than the upper one. This is most likely due to variation in the surface finish between the upper and lower rails or the difference in the compressive force applied between the upper and lower Wedgelock card retainers. A higher compressive force will make better thermal contact, reducing the contact resistance, thereby enhancing the heat flow to that rail.

Card B had a tighter grouping of temperatures over the card surface of a little over 1 °C, as seen in Figure 24. This is near the inherent error of the thermocouple measurements of ±1 °C, indicating that the card temperature was fairly uniform throughout the test.
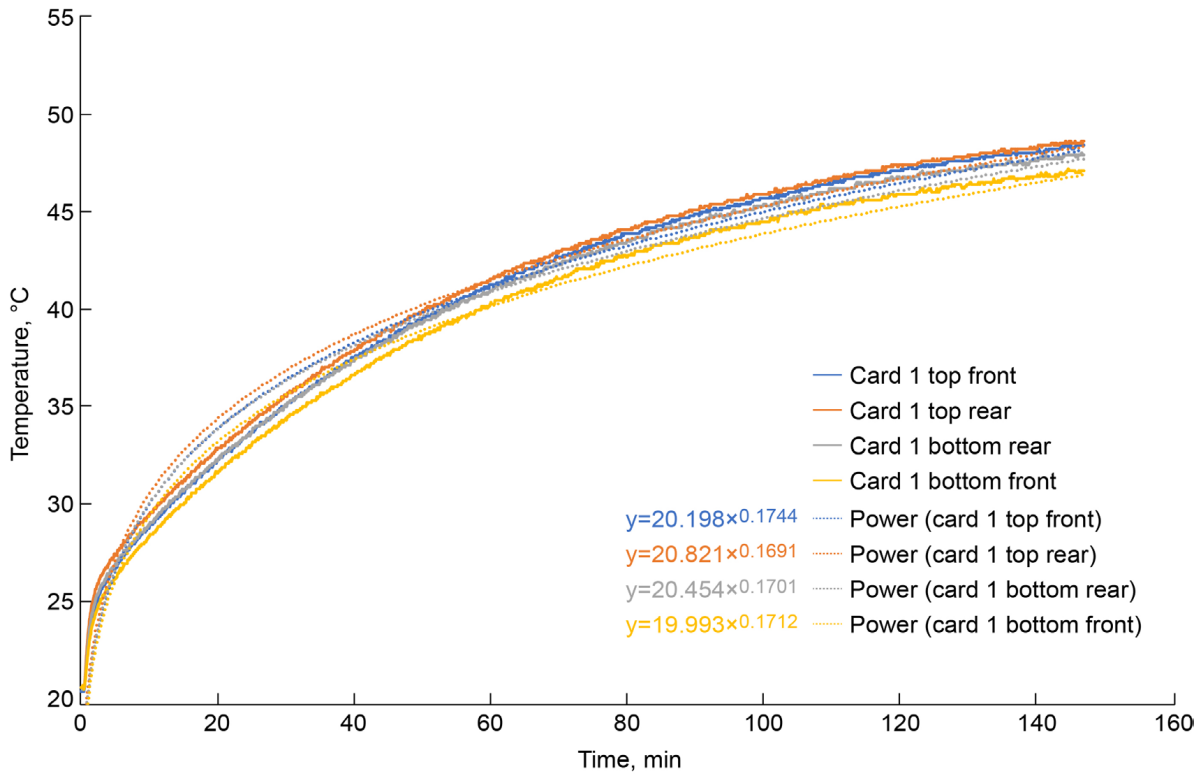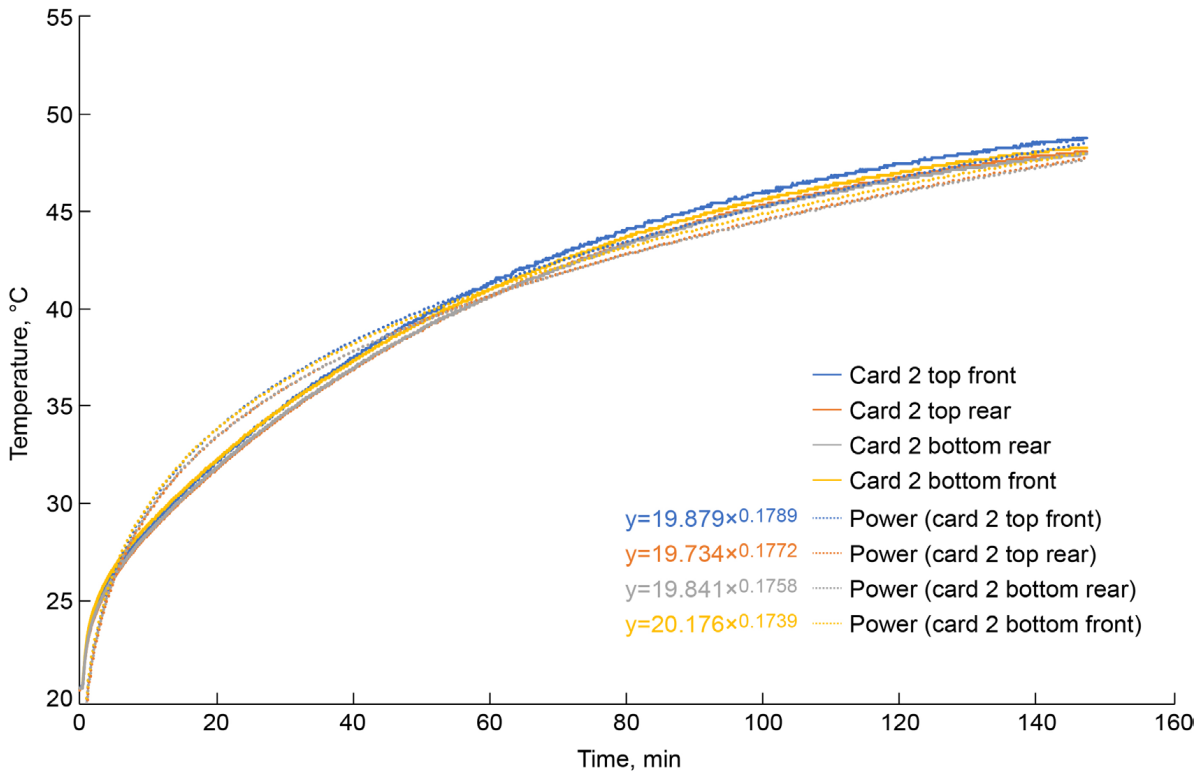
Figure 23.—Case 2 card A temperature versus time.

$y = 20.198 x^{0.1744}$ ...... Power (card 1 top front)
$y = 20.821 x^{0.1691}$ ...... Power (card 1 top rear)
$y = 20.454 x^{0.1701}$ ...... Power (card 1 bottom rear)
$y = 19.993 x^{0.1712}$ ...... Power (card 1 bottom front)



Figure 24.—Case 2 card B temperature versus time.

$y = 19.879 x^{0.1789}$ ...... Power (card 2 top front)
$y = 19.734 x^{0.1772}$ ...... Power (card 2 top rear)
$y = 19.841 x^{0.1758}$ ...... Power (card 2 bottom rear)
$y = 20.176 x^{0.1739}$ ...... Power (card 2 bottom front)

For card C, shown in Figure 25, the temperature measurements of the top thermocouples increased throughout the test as would be expected and were within the measurement error of each other. However, as seen with the case 1 test, the bottom thermocouples varied significantly from each other as well as from the upper thermocouple measurements. There was a step change in their temperature reading toward the end of the test, which brought them in line with the upper thermocouple measurements. The initial variation in these thermocouple measurements was likely due to poor contact between the thermocouple and the card thermal plane or a bad connection of the thermocouples to the data acquisition system. The step change that brought the output in line with the upper thermocouples could have been due to thermal expansion of the card cover, causing improved contact with the thermocouple or a slight movement of the wires, causing a better signal to the data acquisition system. In any case, since the output of these thermocouples was not representative of the actual temperatures on the card, their output was not used to calculate the card average temperature and curve fits to extrapolate the data to estimate the steady-state temperature were not made.

For card D, shown in Figure 26, the temperature distribution over the card was fairly uniform with a 2 °C variation. The highest temperature occurred at the top rear with the lowest at the top front. This indicates a variation in the contact resistance of the upper portion of the card to the support rail, while the front of the card had better contact and lower resistance than the back portion of the card.

As with case 1, the temperatures of the cold plate and case were also monitored. These are shown in Figure 27 and the average values during the estimated steady-state temperature operation are shown in Table V. The cold plate temperature was similar between the upper and lower thermocouples. The cold plate temperature rose approximately 1 °C during the test to an average operating temperature of 21.2 °C. The case had a fairly large variation of 6.3 °C between the front of the case, furthest from the cold plate, to the rear, with an average estimated steady-state temperature of 44.2 °C.
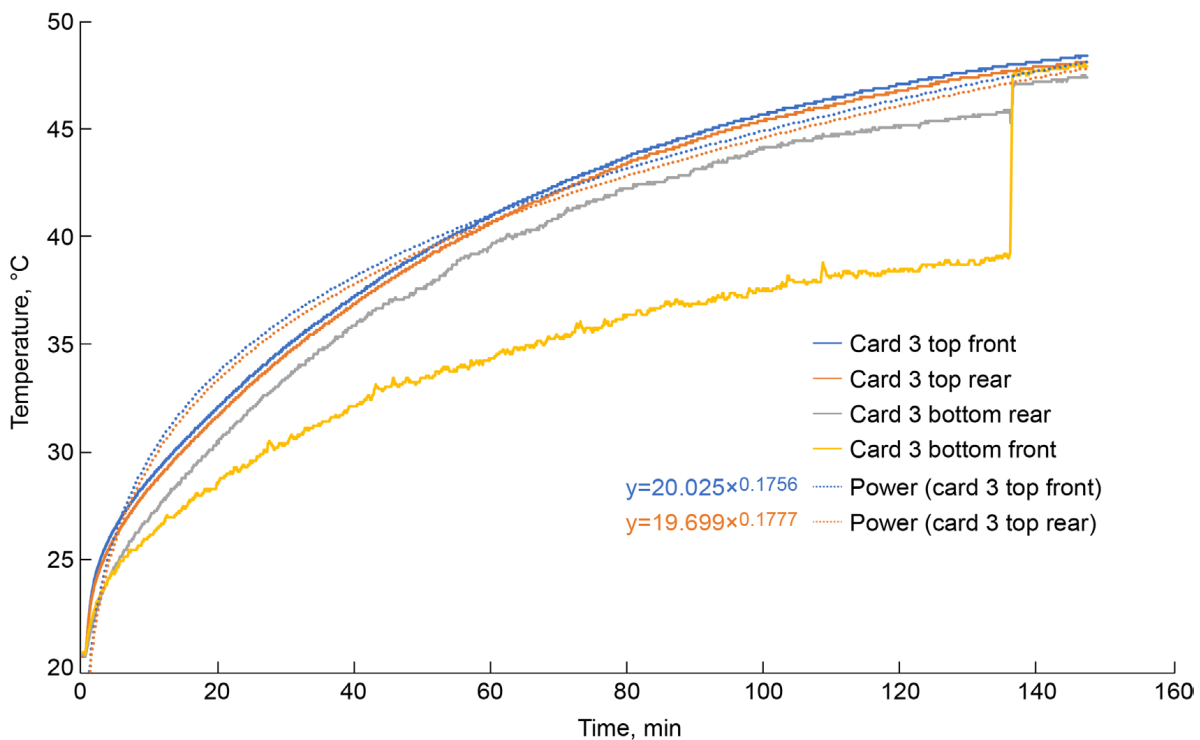


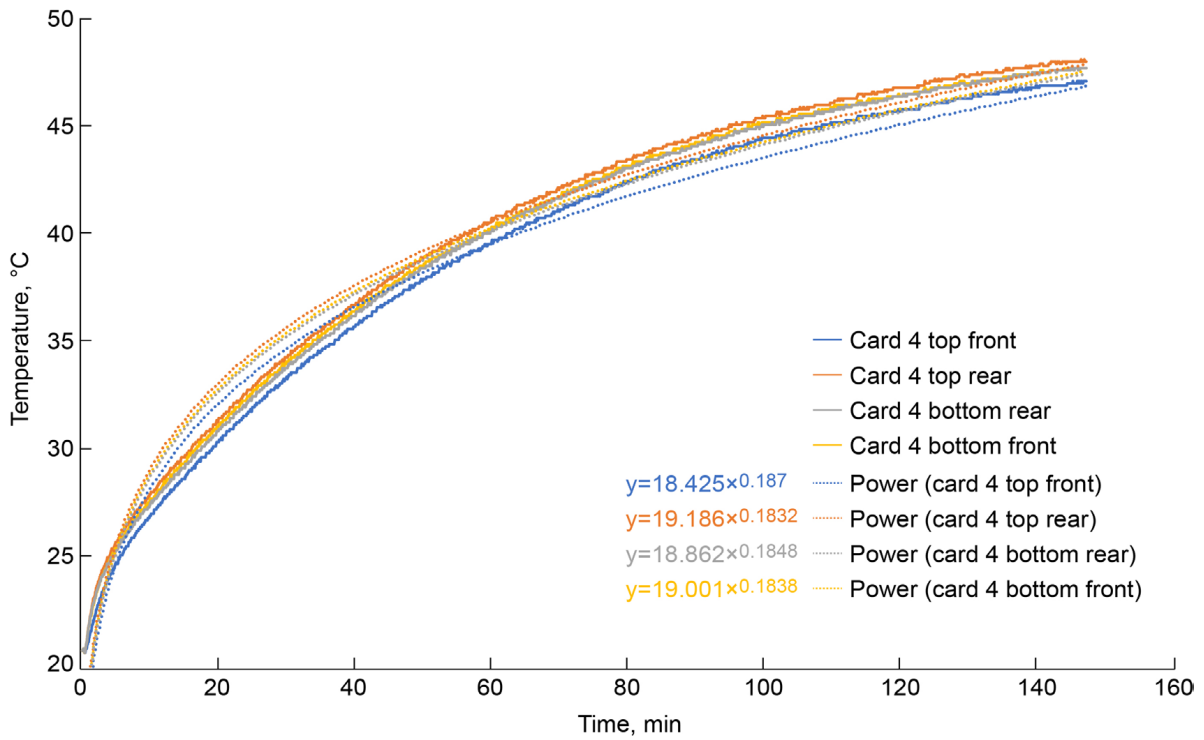Figure 25.—Case 2 card C temperature versus time.

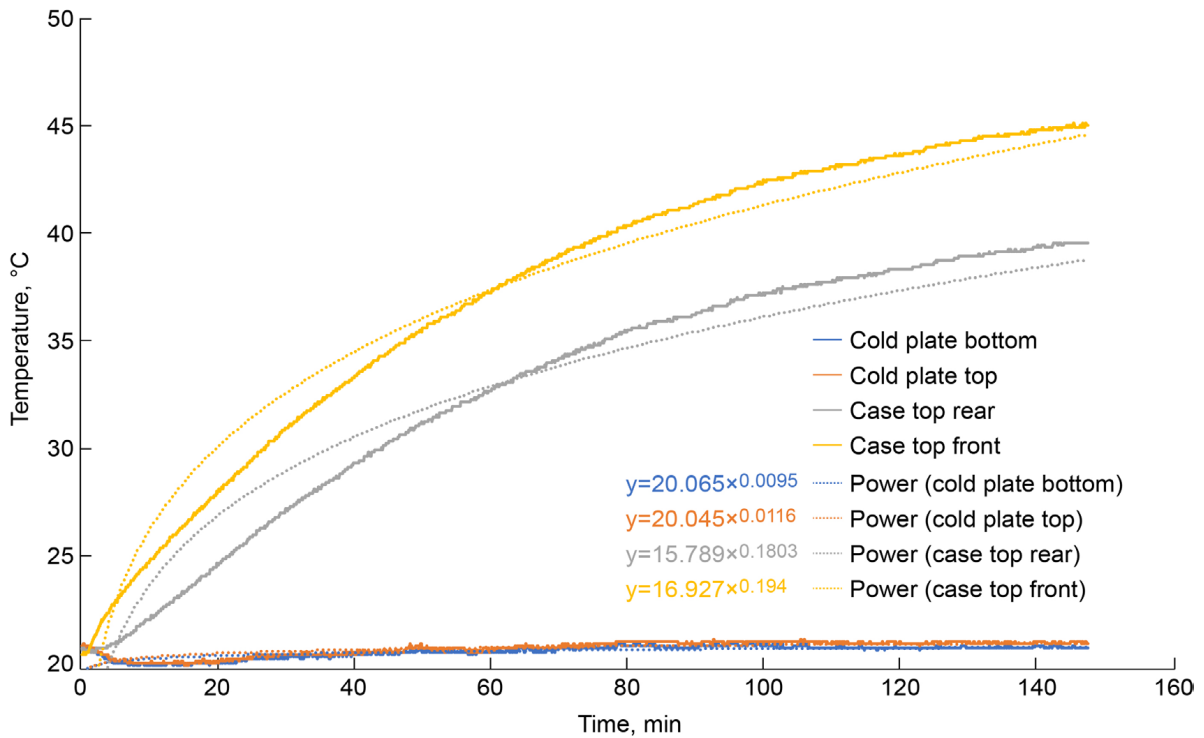Figure 26.—Case 2 card D temperature versus time.



Figure 27.—Case 2 enclosure and cold plate temperatures.

### 3.3 Case 3 Experimental Test Results

In order to reduce the card and case temperature from the levels seen in case 3, Arctic Silver® 5 thermal contact paste was used to increase the thermal contact resistance between the conductive aluminum blocks and the case. The thermal compound was applied and spread over the portion of the case that is in contact with the conductive aluminum blocks, as shown in Figure 28. The conductive blocks were then bolted back onto the case, spreading out the thermal compound, as shown in Figure 29, which reduced the thermal contact resistance between the case and blocks. The Arctic Silver® 5 thermal compound is composed of silver, boron nitride, zinc oxide, and aluminum oxide particles suspended in an ester oil blend. The compound has a measured thermal conductivity of 0.94 W/mK (Ref. 2).

The test results for this case are shown in Figure 30 to Figure 33 for test cards A through D, respectively. The graphs show the rise in temperature of the cards over time as a constant heat load of 16.6 W per card from the heaters is applied. In case 1, the steady-state temperature distribution was reached after approximately 140 min, which is similar to the time needed to reach steady state for case 3. This is less time than that for case 2, which took an estimated 180 min to reach steady-state conditions. The reduced time needed to reach the steady-state condition over case 2 was due to the increased thermal conduction between the case and the conductive blocks.

The estimated steady-state temperature distribution for all four cards, the cold plate, and the case is given in Table VI. These temperatures were averaged from the data after the steady-state conditions were reached, from 140 min through the end of the test.



(a)                                                                                      (b)
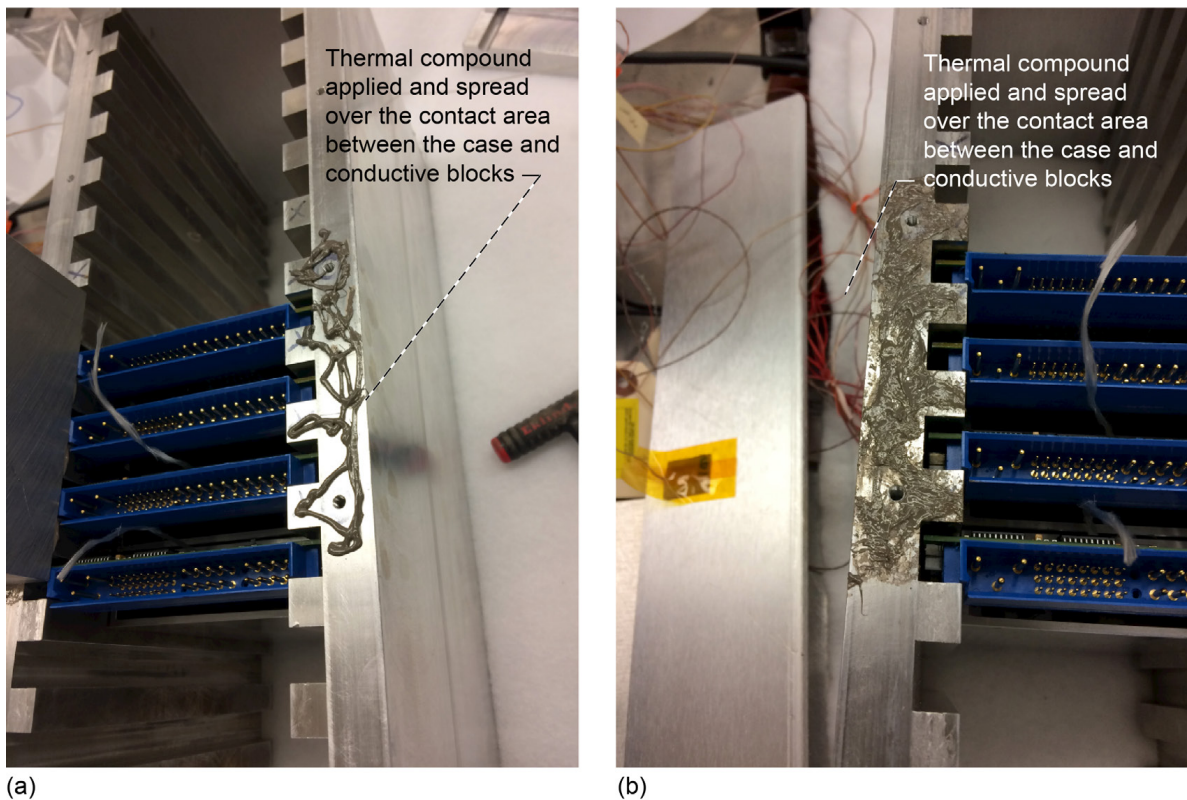
Figure 28.—Application of thermal compound to case. (a) Thermal compound applied to contact area. (b) Thermal compound spread over contact area.
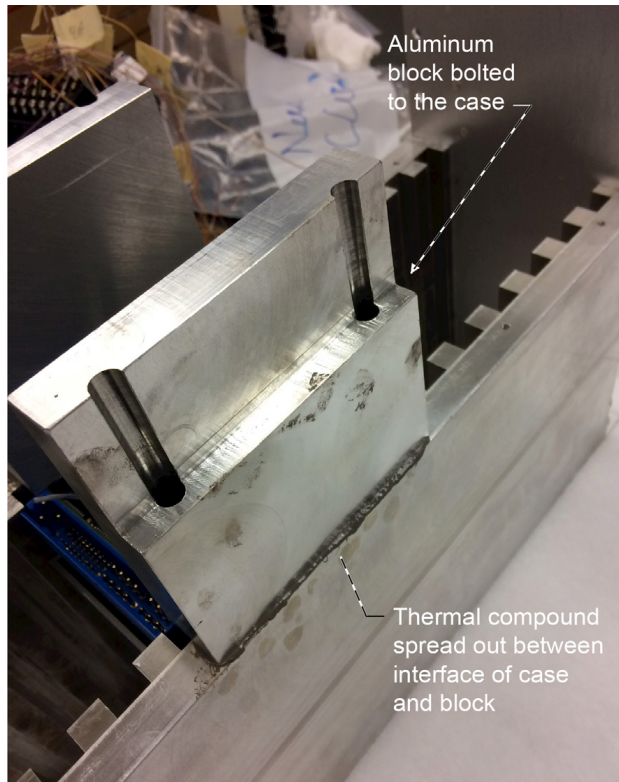
Figure 29.—Thermal compound between block and case.

TABLE VI.—CASE 3 AVERAGE
STEADY-STATE TEMPERATURES

| Location | Average equalization temperature, °C |
|---|---|
| Card A | 43.9 |
| Card B | 44.1 |
| Card C | 43.8 |
| Card D | 43.7 |
| Cold plate, bottom | 21.6 |
| Cold plate, top | 22.0 |
| Case, rear | 36.2 |
| Case, front | 40.8 |

The temperature distribution of card A, given in Figure 30, showed a fairly close temperature distribution over the card with a less than 2 °C variation over the card surface. The bottom front was the coolest and the top rear was the warmest. This could be due to variations in the contact resistance along the support rails and the instrumentation measurement error, which is ±1 °C. One thing to note about the test is that the slope of the temperature curves changes at approximately 107 min into the test. Prior to this, it appears that the system is reaching a steady state and the temperatures begin to level off. Then, they begin to rise again at a higher rate for another 26 min after which they level off at the steady-state values. The reasoning for this change in the heating rate for the cards and the shift to a higher steady-state level is not fully understood. It is probably due to a change in the thermal resistance somewhere along the heat flow path, most likely where the thermal compound was applied at the joint between the case and the

conductive blocks. This change could be due to thermal expansion of the system and a slight loosening of the bolts holding the thermal blocks in place.

The temperature of Card B is given in Figure 31. As with case 2, card B had a tighter grouping of temperatures over the card surface of a little over 1 °C. This is near the inherent error of the thermocouple measurements of ±1 °C, indicating that the card temperature over the card surface was fairly uniform throughout the test. This card also showed a change in heating rate similar to card A. Because multiple cards were affected in the same manner, this strengthens the conjecture that a change in thermal resistance was the cause.

For card C, shown in Figure 32, the temperature measurements of three of the thermocouples varied less than 1 °C and were well within the measurement error of each other. However, as seen with the previous cases, the bottom rear thermocouples varied significantly from the others during the test. This again was likely due to poor contact between the thermocouple and the card thermal plane or a bad connection of the thermocouple to the data acquisition system. Because the output of this thermocouple was likely in error, its output was not used to calculate the card average temperature.

For card D, shown in Figure 33, the temperature distribution over the card was fairly uniform with a 2 °C variation. As with case 2, the highest temperature occurred at the top rear with the lowest at the top front. This indicates a variation in the contact resistance of the upper portion of the card to the support rail where the front of the card had better contact and lower resistance than the back portion of the card.

The temperatures of the cold plate and case were also monitored, as in the previous cases. These are shown in Figure 34 and the average values during the estimated steady-state temperature operation are shown in Table VI. The cold plate temperature was slightly higher for the top thermocouple than the lower. However, this difference is less than 1 °C and could be due to measurement error. The case had a variation of 4.6 °C between the front of the case, furthest from the cold plate, to the rear of the case, with an average estimated steady-state temperature of 38.5 °C. This is 5.7 °C cooler than the previous test without the thermal compound applied between the case and conductive blocks.
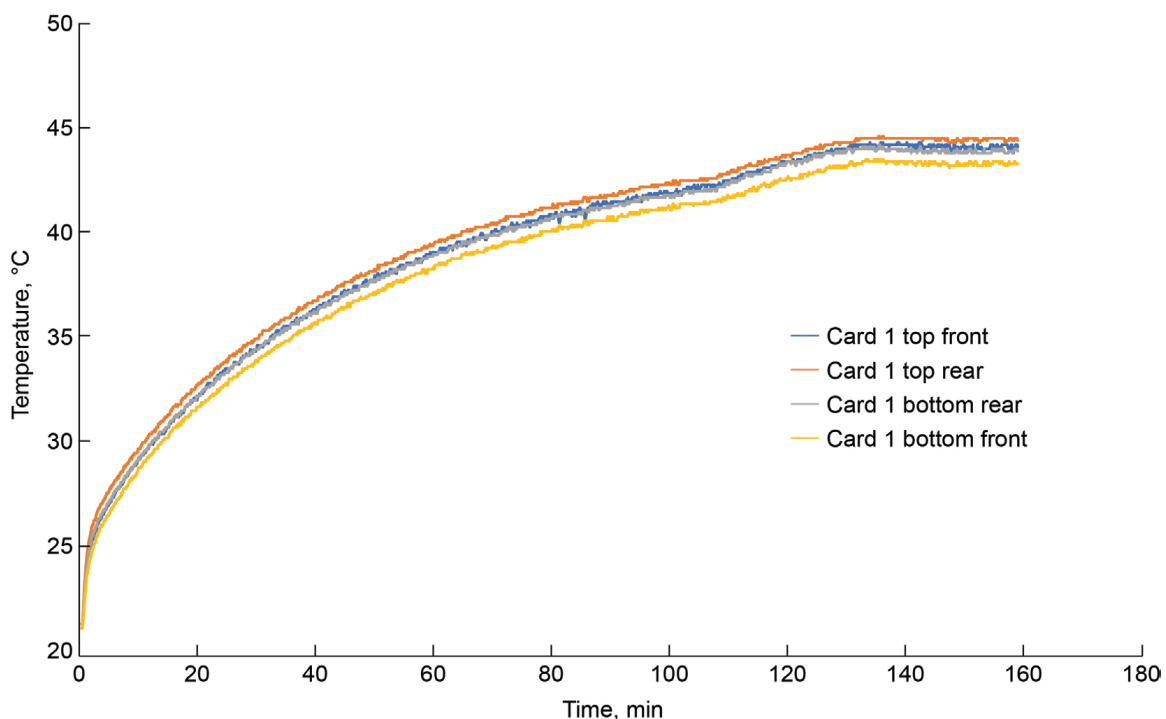


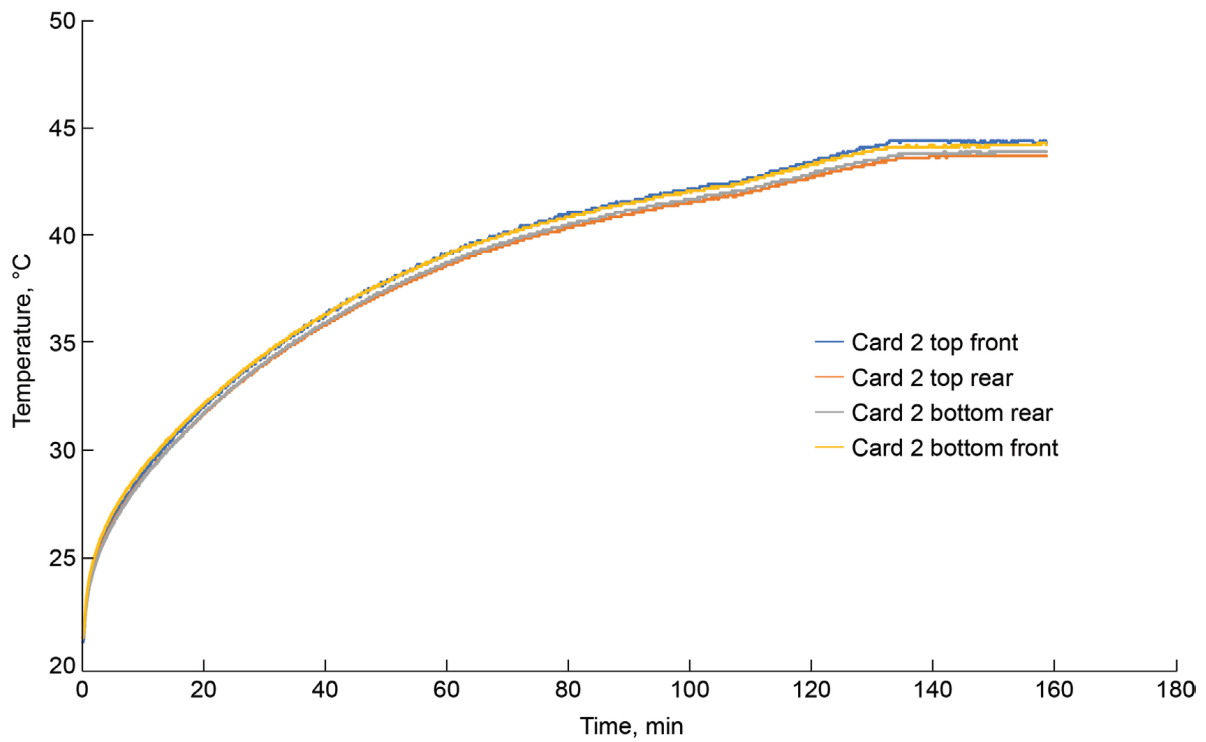Figure 30.—Case 3 card A temperature versus time.

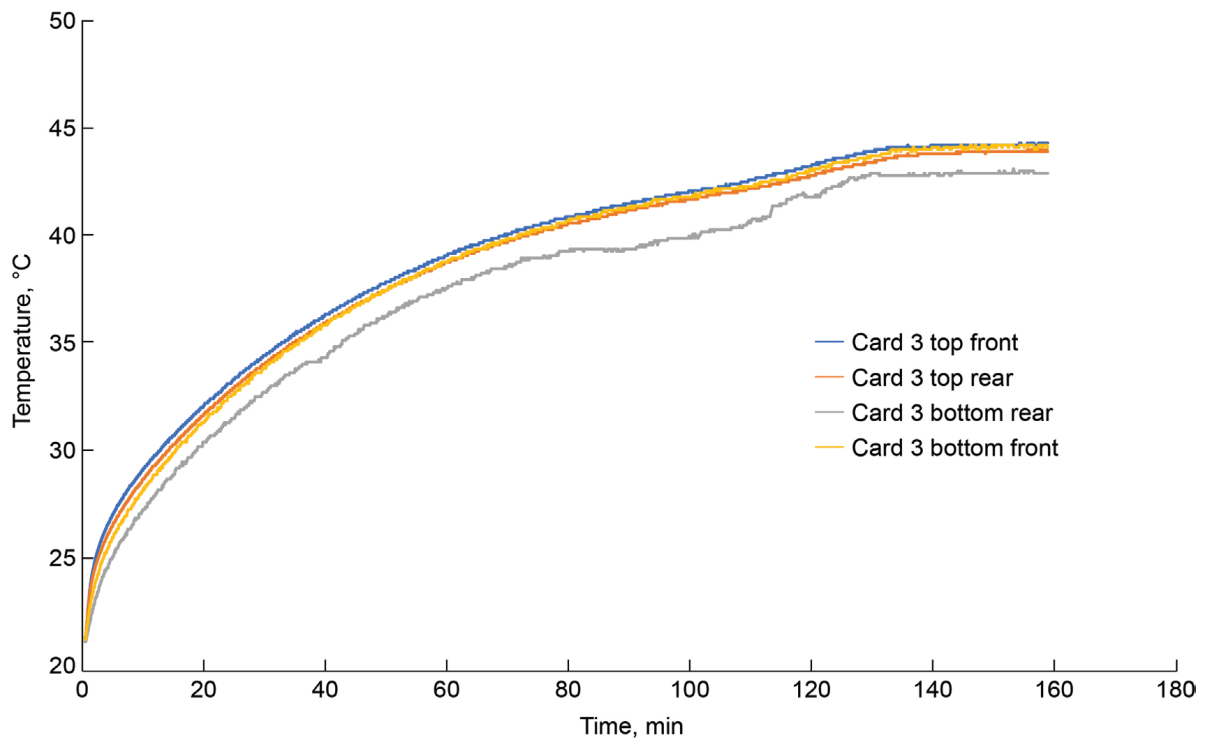Figure 31.—Case 3 card B temperature versus time.

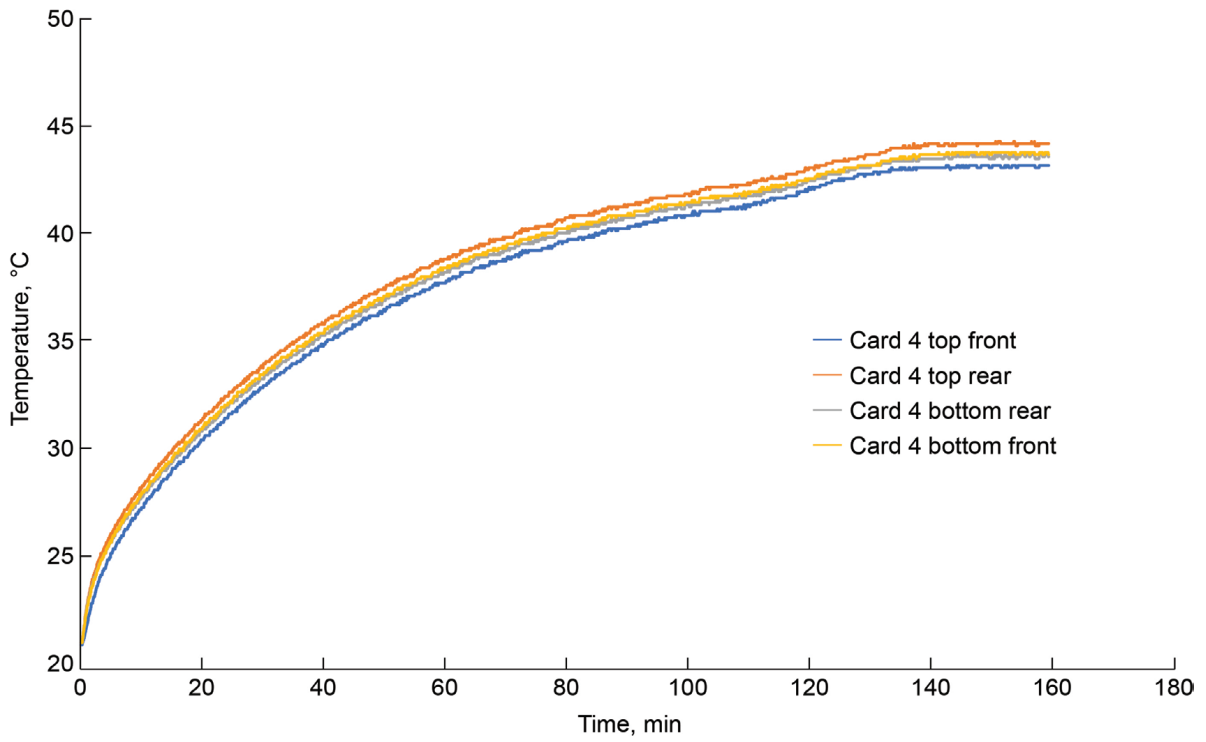

Figure 32.—Case 3 card C temperature versus time.

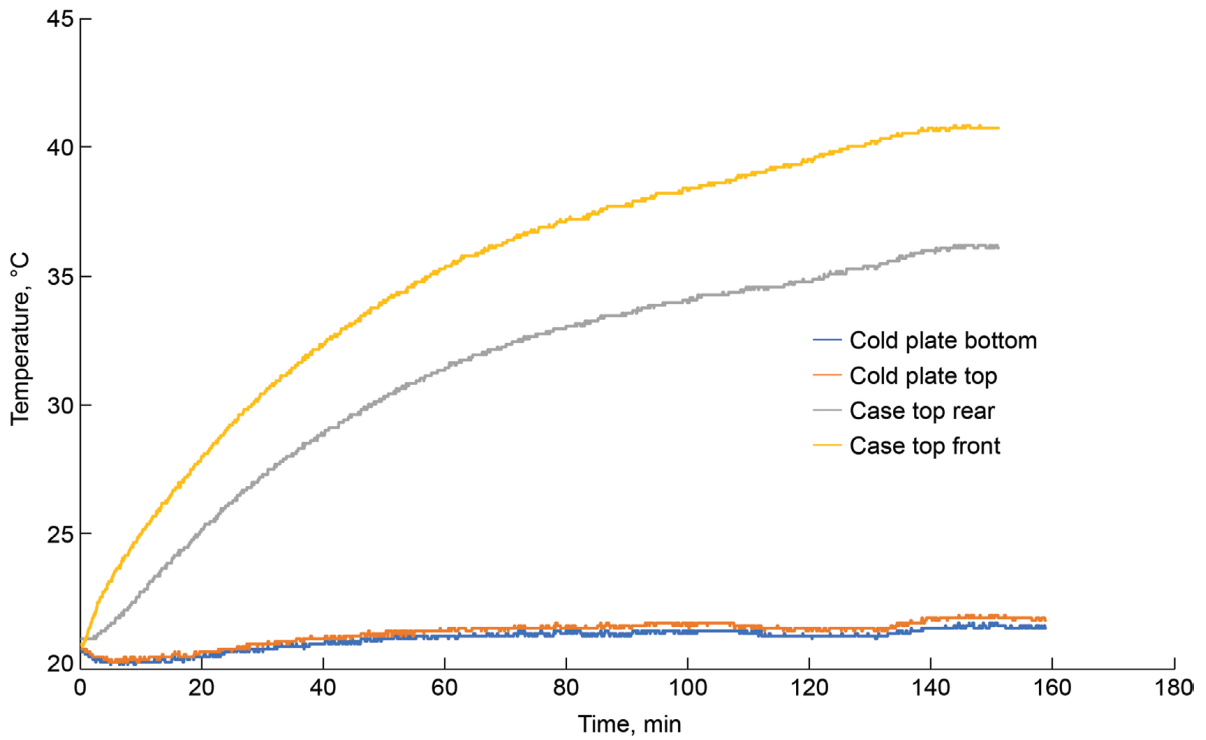Figure 33.—Case 3 card D temperature versus time.



Figure 34.—Case 3 enclosure and cold plate temperatures.

28

## 3.4    Case 4 Experimental Test Results

For the last case, the cold plate was moved to the top of the case and centered over the slots with the four cards installed, as shown in Figure 35. This arrangement provided the shortest heat flow path from the cards to the cold plate and results in the lowest operational temperature. The cold plate was secured to the upper surface of the case with three clamps, similar to how it was secured to the rear of the case. The case thermocouples were moved from the top of the case to the bottom to provide the case temperature during the test. As with the previous cases, the case was fully insulated to minimize any convective heat transfer from its surface to the surroundings during the testing, as shown in Figure 36. This channels almost all of the heat generated by the cards through the case to the cold plate.



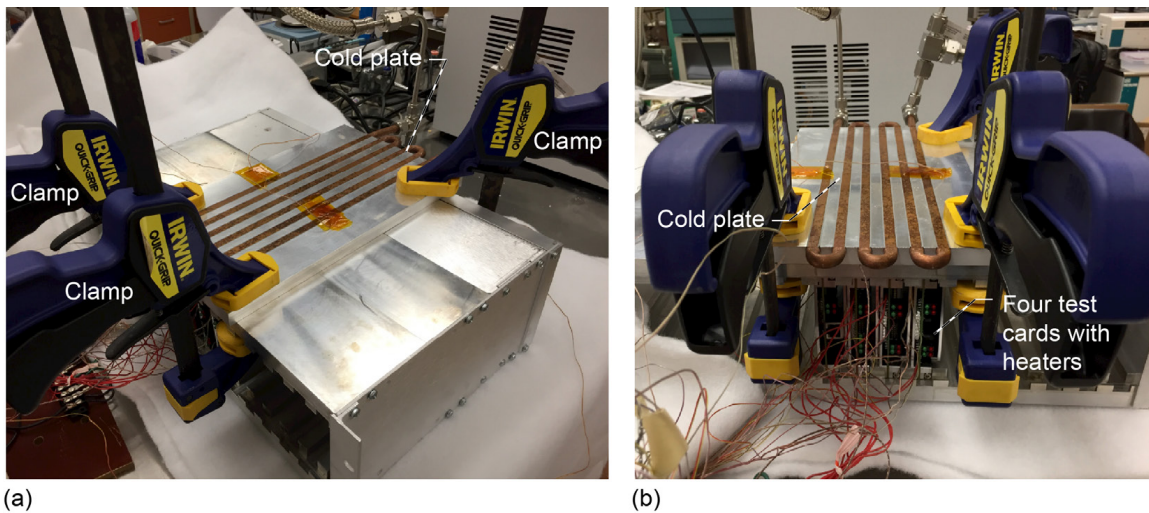(a)                                                              (b)

Figure 35.—Cold plate installed on top of case. (a) Top view of cold plate installed on case. (b) Front view of cold plate installed on case with test card heater wiring connections.



(a)                                                              (b)
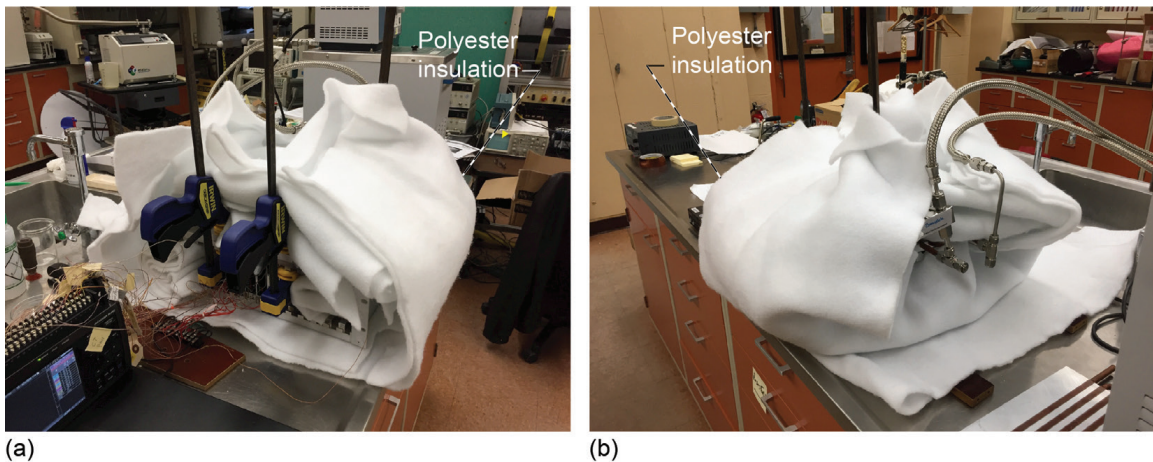
Figure 36.—Case wrapped in insulation for case 4 testing. (a) Front view of insulation wrap installation. (b) Rear view of insulation wrap installation.

The test results for this case are shown in Figure 37 to Figure 40 for the test cards A through D, respectively. The graphs show the rise in temperature of the cards over time as a constant heat load of 16.6 W per card from the heaters is applied. In case 4, the steady-state temperature distribution was reached after approximately 80 min. This is less time than all the previous cases. The reduced time needed to reach the steady-state condition was due to the shorter thermal path between the cards and the cold plate, resulting in a lower overall thermal resistance.

The estimated steady-state temperature distribution for all four cards, the cold plate, and the case is given in Table VII. These temperatures were averaged from the data after the steady-state conditions were reached, from 80 min through the end of the test.

The temperature distribution of card A, given in Figure 37, showed a temperature spread over the card surface of approximately 2 °C. The top front was the coolest and the bottom rear was the warmest. This temperature distribution is what would be expected with the cold plate on the top of the case. The top part of the card should be cooler than the lower part, as is the case.

During the test after a steady state was achieved, there was a gradual temperature drop of approximately 0.5 °C. The temperature then recovered toward the end of the test back to the original steady-state value. The reason for this slight drop is not fully understood. It occurred on all thermocouples, so it was likely due to a change in heat flow from a temporary lowering of the contact resistance between the cold plate and the case or an input power fluctuation to the heaters on the cards.

The temperature of Card B is given in Figure 38. As with card A, there is approximately a 2 °C temperature distribution over the card with the top of the card cooler than the bottom. The temperature difference between the top and bottom of card B is more pronounced than it was for card A and shows a distinct gradient in temperature along the card as heat flows to the cold plate located on the top of the case. Card B also showed a drop and recovery of the card temperature once steady state was reached, as was seen with card A. However, the variation in temperature with card B was much less, approximately 0.2 °C.

For card C, shown in Figure 39, the temperature variation between the top and bottom of the case was approximately 1.5 °C. This is consistent with the variation seen on the other cards tested. However, as seen with the previous cases, the bottom rear thermocouples varied significantly from the others during the test. This again was likely due to poor contact between the thermocouple and the card thermal plane or a bad connection of the thermocouple to the data acquisition system. Because the output of this thermocouple was likely in error, its output was not used to calculate the card average temperature.

TABLE VII.—CASE 4 AVERAGE
STEADY-STATE TEMPERATURES

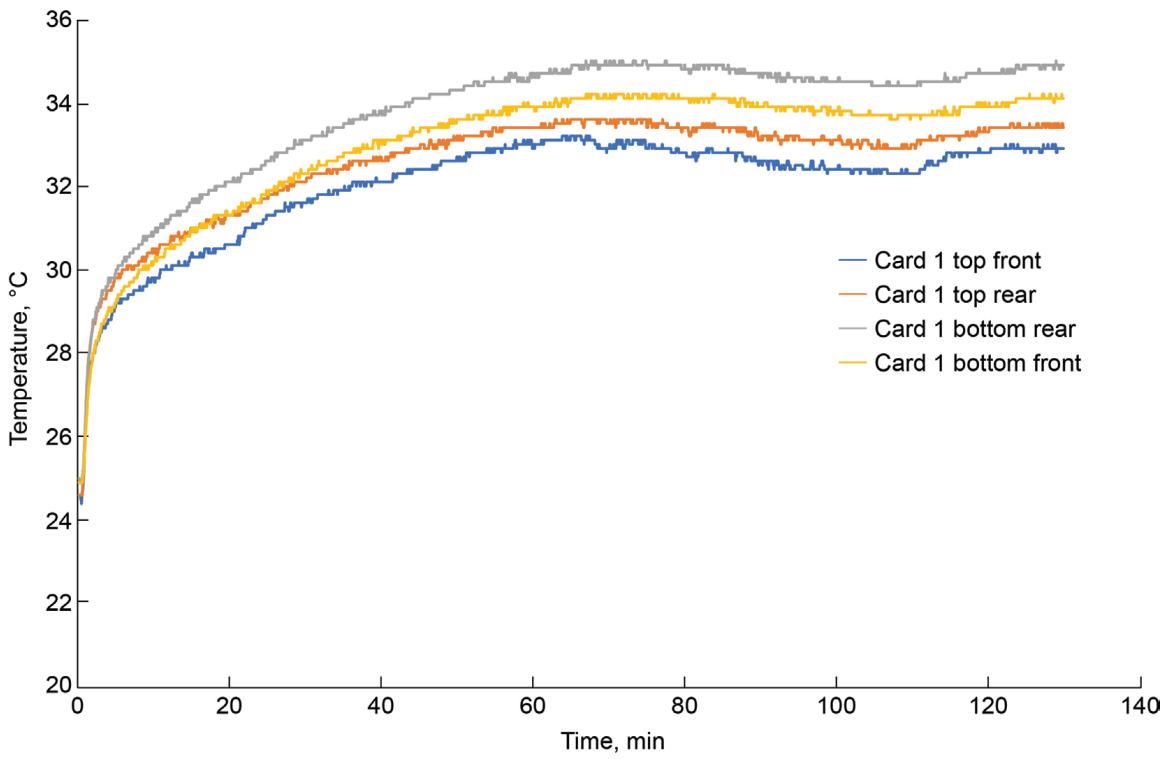| Location | Average equalization temperature, °C |
|---|---|
| Card A | 33.6 |
| Card B | 33.3 |
| Card C | 32.1 |
| Card D | 32.5 |
| Cold plate, left | 21.4 |
| Cold plate, right | 22.1 |
| Case, rear | 32.5 |
| Case, front | 32.9 |

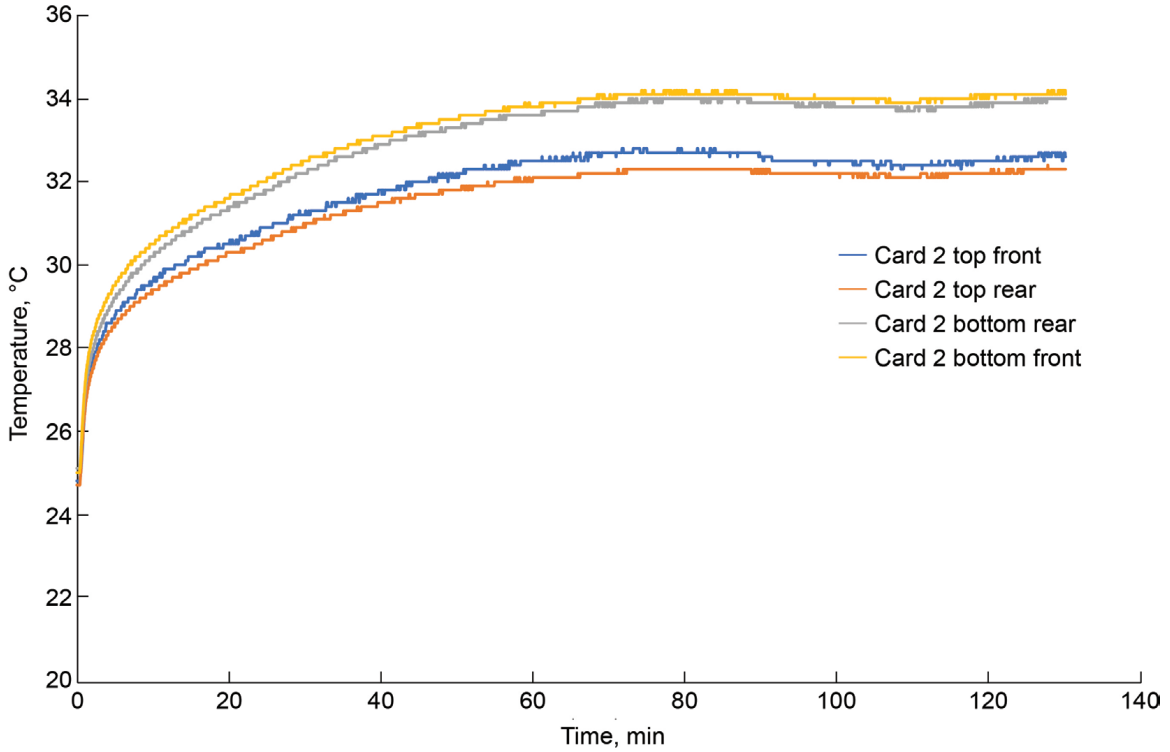Figure 37.—Case 4 card A temperature versus time.



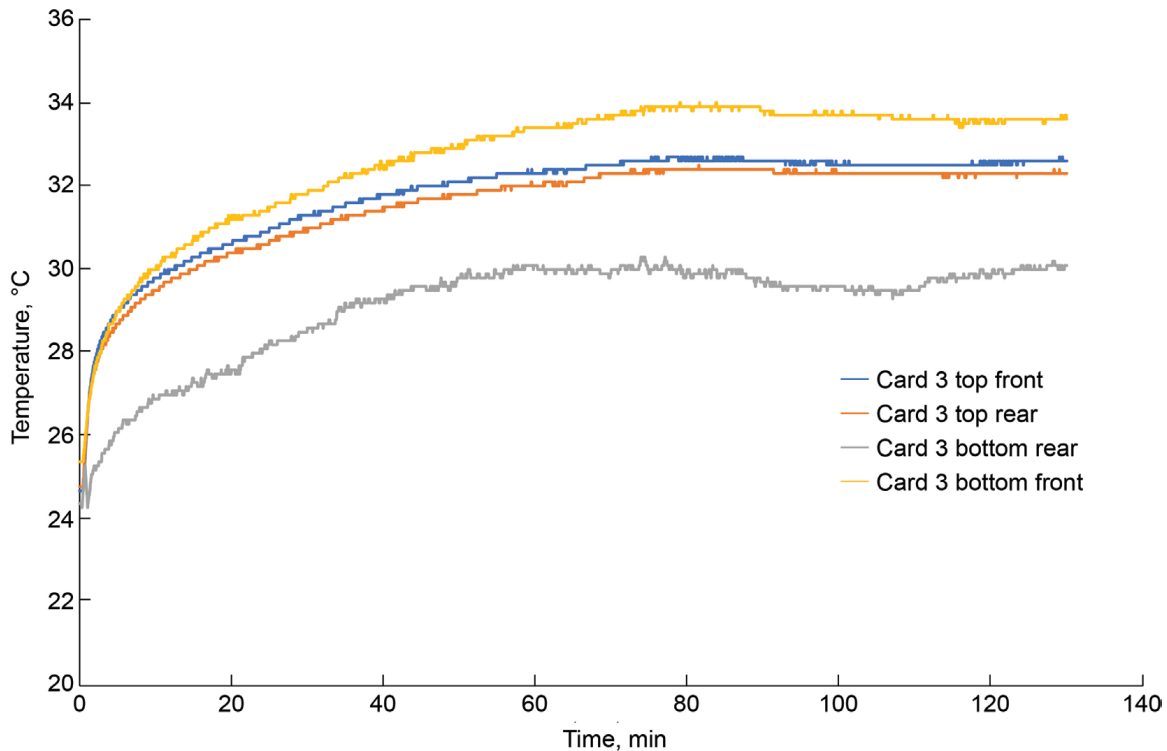Figure 38.—Case 4 card B temperature versus time.

Figure 39.—Case 3 card C temperature versus time.

The temperature distribution for card D, shown in Figure 40, followed a similar pattern to that seen in card A. The overall card temperature distribution was a little greater than 2 °C, and there was a variation between the front and rear thermocouples, where the front was slightly warmer than the rear. Since this gradient between the front and rear thermocouples was evident on cards A and D, it was most likely due to their position at the ends of the four filled card slots. Having an empty slot next to those cards could have influenced their temperature distribution from the front of the case to the rear.

As with the previous cases, the temperatures of the cold plate and case were also monitored. These temperatures are shown in Figure 41 and the average steady-state values for each location are given in Table VII. The cold plate temperature was slightly higher for the left thermocouple than the right. This is likely caused by the left thermocouple being located close to the output from the cold plate back to the chiller and the right thermocouple being located closer to the input from the chiller. However, this difference is less than a degree and could also be due to measurement error. The case had a slight variation of approximately 0.4 °C between the front and rear of the case, which is within the measurement error. Since the cold plate was located on the top of the case, it would be expected that the gradient over the case surface would be minimal.

## 3.5    Combined Case Results

The temperature results for all four cases are summarized in Figure 42 and Table VIII. Figure 42 shows the average card temperature determined during the experiments as well as the temperatures calculated through the analysis. The temperatures predicted through the analysis were very close to those determined through the experiment for cases 2, 3, and 4 with a variation of less than 1 percent for each case. However, the variation in the predicted analysis temperature and the experimental temperature for case 1 varied by over 12 percent.
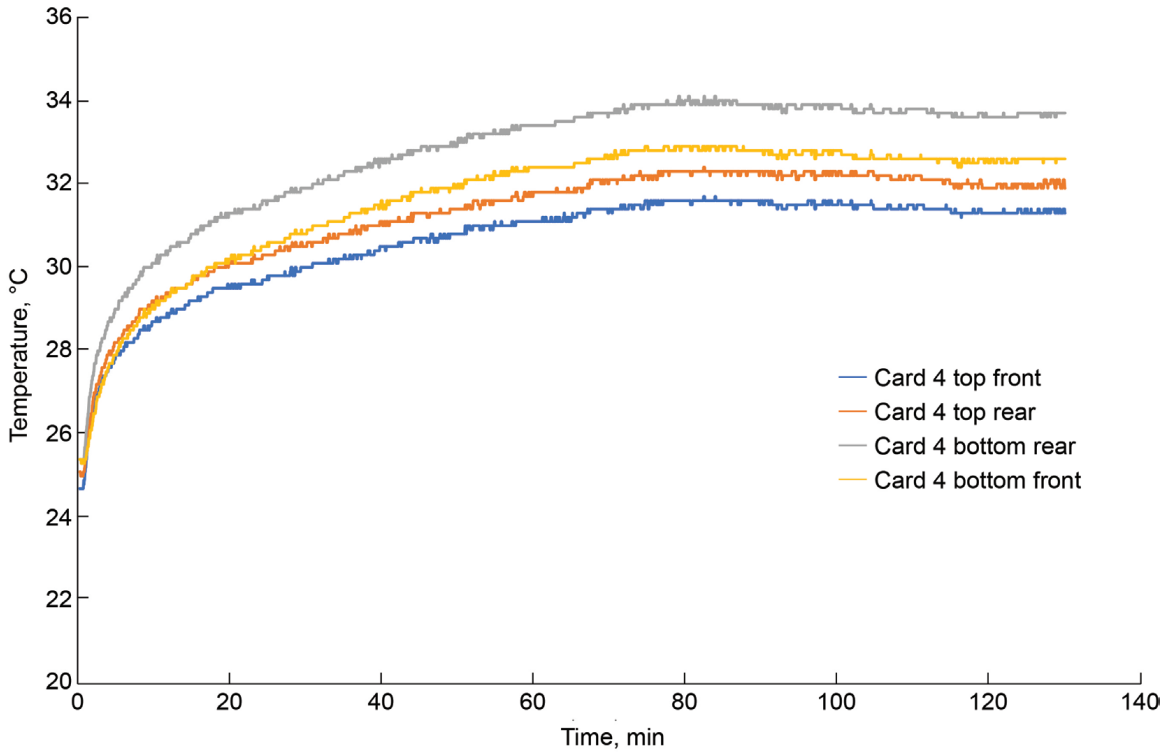
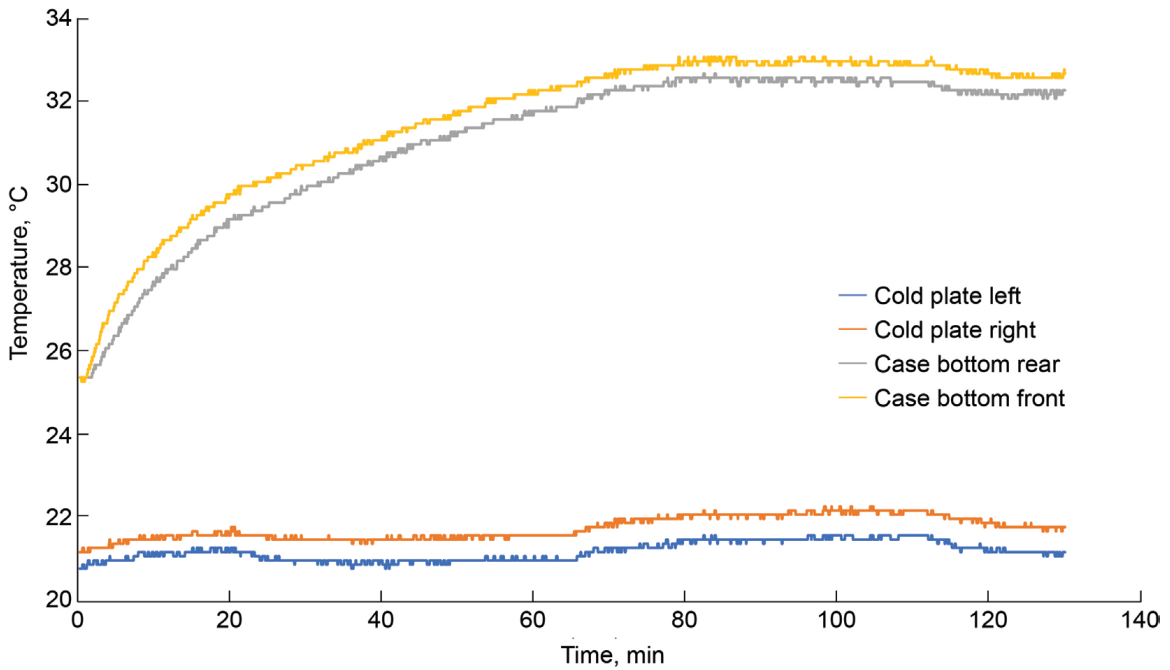Figure 40.—Case 3 card D temperature versus time.



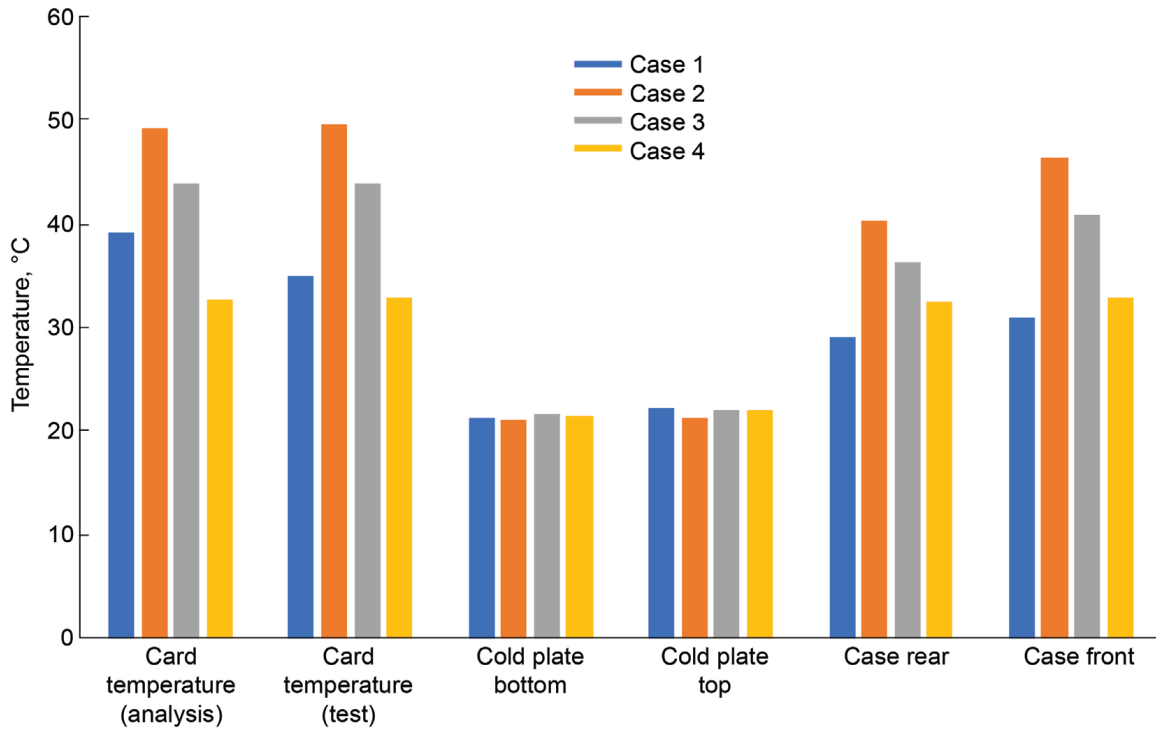Figure 41.—Case 4 enclosure and cold plate temperatures.

Figure 42.—Steady-state temperature comparison between all four cases and analysis.

TABLE VIII.—COMPARISON BETWEEN ANALYSIS AND
EXPERIMENTAL STEADY-STATE CARD TEMPERATURES

|  | Case 1 | Case 2 | Case 3 | Case 4 |
|---|---|---|---|---|
| Analysis steady-state temperature, °C | 39.2 | 49.1 | 43.9 | 32.7 |
| Experimental steady-state temperature, °C | 34.9 | 49.6 | 43.8 | 32.9 |
| Difference between analysis and test data, °C | 4.29 | −0.056 | 0.497 | 0.234 |
| Percent difference between analysis and test, percent | 12.32 | −0.91 | 0.06 | −0.53 |

## 4.0    Conclusions

The reason for the larger variation between the analysis and results for case 1 was most likely due to an overestimate of the contact resistance between the cold plate and the case. For cases 2 and 3, the cold plate was mounted against the conductive blocks and the contact resistance used in the analysis seemed to match well with that interface. However, for case 1, the cold plate was mounted directly to the rear of the case. Since the materials were the same, the same contact resistance was used for cases 1, 2, and 3. Although, the contact resistance between the case and cold plate was most likely much less in case 1 than that for the conductive blocks and the cold plate as modeled in cases 2 and 3.

The lowest card temperatures were achieved for case 4 where the cold plate was located on top of the case. Case 1 had the lowest temperature for all of the cases where the cold plate was located at the rear. This indicates that reducing the distance to the cold plate as well as eliminating material joints can significantly reduce the operating temperature of the cards. Case 3 also showed a significant reduction in the card temperature over case 2. This reduction was achieved by the addition of the thermal compound between the conductive blocks and the case. This reduction illustrates the benefits of good thermal contact between the components in the system in reducing the operation temperature of the cards.

# Appendix—Nomenclature

AMPS  advanced modular power system
PCB    printed circuit board
PDU   power distribution unit

## Symbols

$A_c$      electronics components' contact area to thermal plane
$A_r$      contact surface area between thermal plane and support rails
$A_{rcs}$   cross-sectional area of rails and portion of case associated with heat transfer from one card
$d_p$      average distance from center of thermal plane to support rail
$d_r$      average distance of backplane to center of electronics card
$k_p$      thermal conductivity of thermal plane
$k_r$      thermal conductivity of support rail and case
$L_{be}$    backplane thermal extension length
$L_p$      thermal plane length
$P$       waste heat generated by board
$R_{be}$    thermal resistance for heat conducted through backplane extension to cold plate
$R_{be,cp}$  thermal resistance associated with contact between backplane extension and cold plate
$R_{c(be,cp)}$ contact conductance between backplane extension or support rails and case and cold plate
$R_{c(c,p)}$  contact conductance between electronic components and thermal plane
$R_{c(p,r)}$  contact conductance between thermal plane and support rails
$R_{c(r,be)}$  contact conductance between support rails and backplane extension
$R_{c(r,cp)}$  contact conductance between support rails and case to cold plate
$R_{c,p}$   thermal resistance for heat flow from electronics components to conductive plane
$R_p$     thermal resistance for heat conducted from thermal plane to upper and lower rails
$R_{p,r}$   thermal resistance associated with contact between thermal plane and support rail
$R_r$     thermal resistance for heat conducted down rails and case to backplane of case
$R_{r,be}$   thermal resistance associated with contact between support rail and case and backplane extension
$R_{r,cp}$   contact resistance between cold plate and top of case
$R_{tot}$   sum of thermal resistances between chip surface and heat sink
$T_c$     chip temperature
$T_s$     cold plate temperature
$t_c$      thickness of case
$t_p$      thermal plane thickness
$t_r$      thickness of support rail
$w_c$     width of case section
$w_r$     width of support rail

# References

1. Yovanovich, M.M.: Thermal Interface (Joint) Conductance and Resistance. ECE 309, Contweb.TEX, 1998.
2. Narumanchi, S., et al.: Thermal Interface Materials for Power Electronics Applications. NREL/CP–540–42972, 2008.